
Article:
Sherwen, T. orcid.org/0000-0002-3006-3876, Evans, M. J. orcid.org/0000-0003-4775-032X, Carpenter, L. J. orcid.org/0000-0002-6257-3950 et al. (11 more authors) (2016) Iodine's impact on tropospheric oxidants:A global model study in GEOS-Chem. Atmospheric Chemistry and Physics. pp. 1161-1186. ISSN: 1680-7324

https://doi.org/10.5194/acp-16-1161-2016

Atmos. Chem. Phys., 16, 1161–1186, 2016
www.atmos-chem-phys.net/16/1161/2016/
doi:10.5194/acp-16-1161-2016

Atmospheric Chemistry and Physics
Open Access
EGU

Iodine's impact on tropospheric oxidants: a global model study in GEOS-Chem

T. Sherwen[1], M. J. Evans[1,2], L. J. Carpenter[1], S. J. Andrews[1], R. T. Lidster[1], B. Dix[3], T. K. Koenig[3,4], R. Sinreich[3], I. Ortega[3,4], R. Volkamer[3,4], A. Saiz-Lopez[5], C. Prados-Roman[5], A. S. Mahajan[6], and C. Ordóñez[7]

[1]Wolfson Atmospheric Chemistry Laboratories (WACL), Department of Chemistry, University of York, York, YO10 5DD, UK
[2]National Centre for Atmospheric Science (NCAS), University of York, York, YO10 5DD, UK
[3]Department of Chemistry and Biochemistry, University of Colorado, Boulder, CO 80309-0215, USA
[4]Cooperative Institute for Research in Environmental Sciences, University of Colorado, Boulder, CO 80309-021, USA
[5]Department of Atmospheric Chemistry and Climate, Institute of Physical Chemistry Rocasolano, CSIC, Madrid, 28006, Spain
[6]Indian Institute of Tropical Meteorology, Maharashtra, 411008, India
[7]Met Office, FitzRoy Road, Exeter, EX1 3PB, UK

Correspondence to: T. Sherwen (ts551@york.ac.uk)

Received: 29 June 2015 – Published in Atmos. Chem. Phys. Discuss.: 5 August 2015
Revised: 12 January 2016 – Accepted: 21 January 2016 – Published: 2 February 2016

Abstract. We present a global simulation of tropospheric iodine chemistry within the GEOS-Chem chemical transport model. This includes organic and inorganic iodine sources, standard gas-phase iodine chemistry, and simplified higher iodine oxide (I_2O_X, $X = 2$, 3, 4) chemistry, photolysis, deposition, and parametrized heterogeneous reactions. In comparisons with recent iodine oxide (IO) observations, the simulation shows an average bias of $\sim +90$ % with available surface observations in the marine boundary layer (outside of polar regions), and of $\sim +73$ % within the free troposphere (350 hPa $< p <$ 900 hPa) over the eastern Pacific. Iodine emissions (3.8 Tg yr^{-1}) are overwhelmingly dominated by the inorganic ocean source, with 76 % of this emission from hypoiodous acid (HOI). HOI is also found to be the dominant iodine species in terms of global tropospheric I_Y burden (contributing up to 70 %). The iodine chemistry leads to a significant global tropospheric O_3 burden decrease (9.0 %) compared to standard GEOS-Chem (v9-2). The iodine-driven O_X loss rate[1] (748 Tg O_X yr^{-1}) is due to photolysis of HOI (78 %), photolysis of OIO (21 %), and reaction between IO and BrO (1 %). Increases in global mean OH concentrations (1.8 %) by increased conversion of hydroperoxy radicals exceeds the decrease in OH primary production from the reduced O_3 concentration. We perform sensitivity studies on a range of parameters and conclude that the simulation is sensitive to choices in parametrization of heterogeneous uptake, ocean surface iodide, and I_2O_X ($X = 2$, 3, 4) photolysis. The new iodine chemistry combines with previously implemented bromine chemistry to yield a total bromine- and iodine-driven tropospheric O_3 burden decrease of 14.4 % compared to a simulation without iodine and bromine chemistry in the model, and a small increase in OH (1.8 %). This is a significant impact and so halogen chemistry needs to be considered in both climate and air quality models.

1 Introduction

The chemistry of the troposphere controls the concentration of a range of climate gases including ozone (O_3) and methane (CH_4) (Kim et al., 2011; Voulgarakis et al., 2013;

[1]Here O_X is defined as $O_3 + NO_2 + 2NO_3 + PAN + PMN + PPN + HNO_4 + 3N_2O_5 + HNO_3 + BrO + HOBr + BrNO_2 + 2BrNO_3 + MPN + IO + HOI + INO_2 + 2INO_3 + 2OIO + 2I_2O_2 + 3I_2O_3 + 4I_2O_4$, where PAN = peroxyacetyl nitrate, PPN = peroxypropionyl nitrate, MPN = methyl peroxy nitrate, and MPN = peroxymethacryloyl nitrate.

Young et al., 2013), and determines human and agriculture exposure to air quality pollutants such as O_3 and aerosols (Ainsworth et al., 2012; Fiore et al., 2012; Fowler et al., 2008). The chemical cycles maintaining concentrations of these atmospheric constituents are complex, and depend strongly upon the concentrations of O_3 and of the hydroxyl radical (OH) as key oxidants. Understanding the budgets and controls on these gases is therefore central to assessments of tropospheric chemistry (Voulgarakis et al., 2013).

The basic chemistry of O_3 and OH in the troposphere is coupled, and the central aspects of this are well known (Young et al., 2013). Over the last decades significant research effort has gone into understanding the production of O_3, typically over continental regions due to its adverse impact on health and food security (Ainsworth et al., 2012; Fowler et al., 2008). However, less emphasis has focused on its chemical destruction. O_3 is chemically lost in the troposphere predominantly through photolysis in the presence of water or its reactions with HO_2 and OH (Lelieveld and Dentener, 2000). However, bromine and iodine compounds have also been identified as additional sinks for O_3 and as perturbations to OH cycling (Chameides and Davis, 1980; von Glasow et al., 2004). Of the two, iodine has arguably the more complex chemistry.

Historically, the dominant source of iodine was thought to be iodinated organic compounds from the ocean (Chuck et al., 2005; Jones et al., 2010; Law and Sturges, 2006). More recently, emission of inorganic halogen compounds (I_2 and HOI) has been identified as a significant source (Carpenter et al., 2013). Our understanding of its chemistry has been described in recent publications (Saiz-Lopez et al., 2012b; Sommariva et al., 2012). Once emitted into the atmosphere, the highly labile iodinated precursors rapidly photolyse with lifetimes of seconds (e.g. I_2/HOI) to days (e.g. CH_3I) to release atomic iodine. The iodine can catalytically destroy O_3 by the reaction of $O_3 + I$ to form IO, followed by secondary reactions ($+HO_2$, $+IO$, $+NO_2$, $+BrO$) which can regenerate atomic I without the abstracted oxygen. For instance IO reacts with HO_2, leading to HOI formation, and this is rapidly photolysed to reform I causing a net conversion of HO_2 to OH.

Much of the uncertainty in iodine chemistry involves the production and fate of their higher oxides (I_2O_X). These higher oxides are formed from a chain reaction of IO self-reactions (Sommariva et al., 2012):

$$O_3 + I \rightarrow IO + O_2 \quad \text{(R1)}$$
$$IO + IO \rightarrow OIO + I \quad \text{(R2)}$$
$$IO + IO \rightarrow I_2O_2 \quad \text{(R3)}$$
$$IO + OIO \rightarrow I_2O_3 \quad \text{(R4)}$$
$$OIO + OIO \rightarrow I_2O_4. \quad \text{(R5)}$$

Due to their short lifetimes and low concentrations, measuring iodine species poses significant challenges and so the observational data set is sparse. For decades, measurements have focused on organic compounds and mainly CH_3I (Saiz-Lopez et al., 2012b). Technique development for in situ measurements has led to an increase in data availability over the last decade, for both organic (e.g. CH_3I and CH_2IX, with $X = Cl, Br, I$) and inorganic (e.g. IO, OIO, I_2) species (Saiz-Lopez et al., 2012b).

Recent measurements from aircraft (Dix et al., 2013; Volkamer et al., 2015; Wang et al., 2015), balloons (Butz et al., 2009), mountain tops (Puentedura et al., 2012), ground stations (Lawler et al., 2014; Mahajan et al., 2010; Read et al., 2008), and cruises (Großmann et al., 2013; Jones et al., 2010; Mahajan et al., 2012) have enabled the development of global organic halogen emissions (Ordóñez et al., 2012; Ziska et al., 2013) and, more recently, data sets of IO observations with extensive geographical coverage (Prados-Roman et al., 2015b; Volkamer et al., 2015; Wang et al., 2015).

Iodine chemistry has been evaluated by a number of box model studies (Sander et al., 1997; Mahajan et al., 2009; McFiggans et al., 2000, 2010; Read et al., 2008; Saiz-Lopez et al., 2007) and a few global model studies (Prados-Roman et al., 2015a; Saiz-Lopez et al., 2012a, 2014). The initial focus was predominantly on geographic regions with elevated concentrations (e.g. polar, Sander et al., 1997; Saiz-Lopez et al., 2007; and coastal, Mahajan et al., 2009; McFiggans et al., 2000; Saiz-Lopez et al., 2006) and attempted to explain localized chemical perturbations mainly through the use of box models.

When considered alongside bromine chemistry, box model studies have shown the magnitude of halogen-driven O_3 loss processes to be up to 45 % (Mahajan et al., 2009; Read et al., 2008) of the total loss. Iodine can change the local HO_2 : OH ratio due to the production of HOI from HO_2 and IO, and its subsequent photolysis to release OH (Bloss et al., 2005a; Chameides and Davis, 1980). Perturbation to the NO : NO_2 ratio has been shown to be significant at higher IO concentrations in polluted coastal locations (McFiggans et al., 2010) due to the ability of IO to oxidize NO into NO_2, which affects O_3 production. More recently, measurements in the marine boundary layer on ground-based island monitoring stations (Read et al., 2008; Mahajan et al., 2010; Gómez Martín et al., 2013), on ships (Großmann et al., 2013; Mahajan et al., 2010; Prados-Roman et al., 2015b), by balloon (Butz et al., 2009), and by aircraft (Dix et al., 2013; Volkamer et al., 2015; Wang et al., 2015) have demonstrated that these O_3 loss processes also occur in remote non-coastal locations.

Recently, the role of reactive halogens have also been investigated in global chemical transport models (Parrella et al., 2012) and chemistry-climate models (Ordóñez et al., 2012; Saiz-Lopez et al., 2014). Inclusion of tropospheric bromine, iodine, and chlorine chemistry into a global model led to significant changes in the composition troposphere. Tropospheric marine average O_3 columns decrease by of the order of ~ 10 % (Saiz-Lopez et al., 2012a, 2014). As in the

box model studies, up to ∼ 30 % of the O_3 loss in the marine boundary layer (900 hPa < p) is found to be driven by halogens (Saiz-Lopez et al., 2012a, 2014). Similarly, high levels of halogen-driven O_3 loss are also found in the upper troposphere (350 hPa > p > tropopause), with lower (10–15 %) impacts in the free troposphere (350 hPa < p < 900 hPa) (Saiz-Lopez et al., 2012a, 2014).

In order to explore our current understanding of the tropospheric chemistry of iodine we present a global modelling study of tropospheric iodine chemistry, using the GEOS-Chem chemical transport model. The new chemistry is described in Sect. 2. Section 3 describes the comparison of modelled iodine concentrations against observations. Then Sect. 4 describes modelled global chemical distributions by family. Impacts on O_3 and OH are described in Sect. 5. In Sect. 6 we consider interactions of iodine with bromine, and in Sect. 7 we look at key sensitivities of the simulation. Section 8 summarizes our conclusions.

2 GEOS-Chem simulation

We use here the GEOS-Chem (http://www.geos-chem.org) chemical transport model version v9-02, with transport driven by assimilated meteorological and surface data fields (GEOS-5) from NASA's Global Modelling and Assimilation Office (GMAO). We have adapted the existing chemistry scheme which includes O_X, HO_X, NO_X, and VOC chemistry as described recently in Mao et al. (2013), bromine chemistry (Parrella et al., 2012), and a mass-based aerosol scheme. Stratospheric chemistry is climatologically represented based on LINOZ McLinden et al. (2000) for O_3 and linearized chemistry is applied for other species with concentrations taken from the Global Modelling Initiative (GMI) as described previously (Murray et al., 2012).

Iodine tracers (I_2, HOI, IO, OIO, HI, INO_2, INO_3, I, INO, CH_3I, CH_2I_2, CH_2IBr, CH_2ICl, I_2O_2, I_2O_3, I_2O_4, and "aerosol iodine") are included in the model. The modelled emissions, deposition, chemistry, photolysis, and aerosol processes of these compounds are described below. No chemical processing of iodine species is performed in the stratosphere.

Notably our work differs from recent global iodine simulations (Saiz-Lopez et al., 2014) in its treatment of I_2O_X ($X = 2, 3, 4$). Our model ("Br+I") considers the photolysis of these compounds whereas their "Base" simulation does not. This leads to our simulations having a more active iodine chemistry and this is discussed in Sect. 2.4.

As well as the core simulation present in this paper ("Br+I"), comparisons with the existing standard GEOS-Chem simulation ("BROMINE") are presented, which includes bromine chemistry as described in Sect. 2.6. When considering the coupling of iodine and bromine, two additional simulations are included, one with just iodine chemistry ("IODINE") and one with no bromine or iodine chemistry ("NOHAL").

Table 1. Total simulated emissions for iodinated species.

Species	Emissions Tg I yr^{-1}
CH_3I	0.26
CH_2I_2	0.11
CH_2ICl	0.18
CH_2IBr	0.05
I_2	0.32
HOI	2.91
Total	3.83

For budgets and general analysis we run the model at $2° \times 2.5°$ resolution for 2 years (2004 and 2005) discarding the first "spin up" year and using the final year (2005) for analysis and budgets. For the sensitivity study (Sect. 7) the model is run with the same period for "spin up" and analysis, but at $4° \times 5°$ resolution. The model output is discussed with focus on the marine boundary layer (900 hPa < p), the free troposphere (350 hPa < p < 900 hPa), and upper troposphere (350 hPa > p > tropopause). Comparisons with observations involve separate spin-up simulations, run with the date-appropriate meteorology, sampled at the spatially and temporally nearest grid box and time step. We report here mixing ratios as pmol mol^{-1} or nmol mol^{-1}, which are equivalent to the more widely used pptv or ppbv.

2.1 Iodine emissions

Both organic and inorganic iodine species (Table 1 and Fig. 1) are emitted into the atmosphere. Monthly emissions of organic iodine compounds (CH_3I, CH_2I_2, CH_2IBr, and CH_2ICl) are taken from Ordóñez et al. (2012) which parametrizes fluxes based on chlorophyll a in the Tropics and constant oceanic fluxes with 2.5 coast-to-ocean emission ratios for extratropical regions, and follows Bell et al. (2002) for CH_3I. Inorganic iodine compounds (HOI, I_2), formed from the uptake of O_3 to the ocean and the subsequent ocean surface reaction of O_3 with iodide (I^-), are emitted as calculated from Eqs. (19) and (20) in Carpenter et al. (2013). We parametrize ocean surface I^- concentration from the sea surface squared temperature relationship in Table 2 from Chance et al. (2014), the O_3 concentration in the lowermost level of the model, and the 10 m wind speed from meteorological fields. The 10 m wind speed used by the parametrization is limited to a minimum of 5 m s^{-1} to prevent unsubstantiated emissions at low wind speeds. Annual average iodine emission fluxes are shown in Fig. 1.

Global emission totals (Table 1) are consistent with recent work (Saiz-Lopez et al., 2014) for organic iodine compounds as they also use Ordóñez et al. (2012). Inorganic

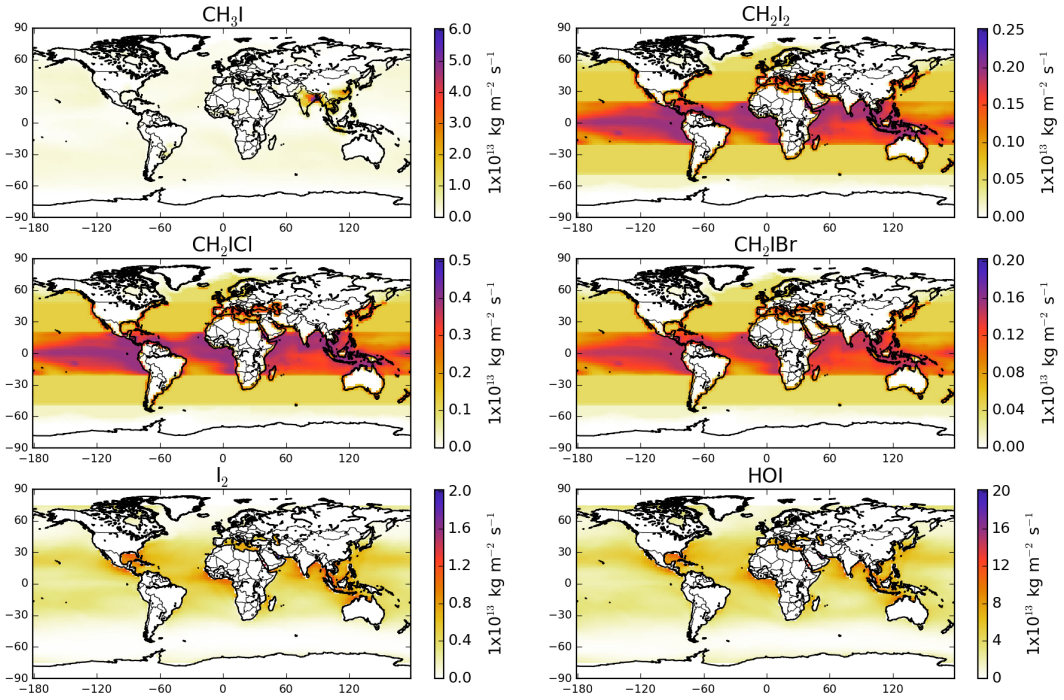

Figure 1. Annual mean surface fluxes for iodine precursors in the "Br+I" simulation in kg m^{-2} s^{-1}.

Table 2. Henry's law coefficients and molar heats of formation of iodine species. Where Henry's law constant equals infinity a very large value is used within the model (1×10^{20} M atm^{-1}). The INO_2 Henry's law constant is assumed equal to that of $BrNO_3$, from Sander (2015), by analogy. For I_2O_X ($X = 2, 3, 4$) a Henry's law constant of infinity is assumed by analogy with INO_3. * Effective Henry's law of HI is calculated for acid conditions through $K^*_H(T) = K_H(T) \times (1 + \frac{K_a}{[H^+]})$, where $K_a = 1 \times 10^9$ M is the acid dissociation constant (Bell, 1973).

Num.	Species	Henry's law constant M atm^{-1}	Reference	Molar heat of formation 298 K/R (K)	Reference
D1	HOI	1.53×10^4	Sander (2015)	-8.37×10^3	Sander et al. (2006)
D2	HI	$2.35 \times 10^{0*}$	Sander (2015)	-3.19×10^3	Sander et al. (2006)
D3	INO_3	∞	Vogt et al. (1999)	-3.98×10^4	Kaltsoyannis and Plane (2008)
D4	I_2O_2	∞	see caption text	-1.89×10^4	Kaltsoyannis and Plane (2008)
D5	I_2	2.63×10^0	Sander (2015)	-7.51×10^3	Sander et al. (2006)
D6	INO_2	3.00×10^{-1}	see caption text	-7.24×10^3	Sander et al. (2006)
D7	I_2O_3	∞	see caption text	-7.70×10^3	Kaltsoyannis and Plane (2008)
D8	I_2O_4	∞	see caption text	-1.34×10^4	Kaltsoyannis and Plane (2008)

fluxes calculated in this study are 47 % higher than in previous work (Saiz-Lopez et al., 2014), despite using the same parametrization (Carpenter et al., 2013; MacDonald et al., 2014). Although model-specific differences exist in sea surface temperatures, 10 m wind speeds, and O_3 concentration, the largest differences lie in the choice of parametrization for sea surface iodide (see Sect. 7.5).

2.2 Iodine deposition

The model's deposition scheme has recently been updated (Amos et al., 2012). Dry deposition of the new iodine compounds is computed via the standard GEOS-Chem implementation of the "resistance-in-series" approach (Wesely, 1989) using literature Henry's law coefficients (Sander, 2015). This approach is applied to I_2, HI, HOI, INO_2, INO_3, I_2O_2, I_2O_3, and I_2O_4. Aerosol iodine is assumed to have the same wet deposition properties as sulfate aerosol.

Wet deposition is calculated for I_2, HI, HOI, INO_2, INO_3, I_2O_2, I_2O_3, and I_2O_4 for both large-scale (frontal) and convective rain by applying scavenging in and below clouds (Liu et al., 2001) using species-specific values for Henry's law coefficients (Sander, 2015; Vogt et al., 1999) and molar heats

Table 3. Bimolecular and unimolecular iodine reactions. These are given in the Arrhenius form with the rate equal to $A \cdot \exp(\frac{Ea}{RT})$. Unknown values are represented by a dash and these set to zero in the model, reducing the exponent to 1. The bimolecular reactions with an M in them represent termolecular reactions where the pressure dependence is not known or are unimolecular decomposition reactions. Reactions included, but not in IUPAC/JPL, are discussed further in Sect. A1.1.

Rxn ID	Reaction	A $\mathrm{cm^3\,molecules^{-1}\,s^{-1}}$	Ea/R K	Citation
M1	$I + O_3 \rightarrow IO + O_2$	2.10×10^{-11}	−830	Atkinson et al. (2007)
M2	$I + HO_2 \rightarrow HI + O_2$	1.50×10^{-11}	−1090	Sander et al. (2011)
M3	$I_2 + OH \rightarrow HOI + I$	2.10×10^{-10}	–	Atkinson et al. (2007)
M4	$HI + OH \rightarrow I + H_2O$	1.60×10^{-11}	440	Atkinson et al. (2007)
M5	$HOI + OH \rightarrow IO + H_2O$	5.00×10^{-12}	–	Riffault et al. (2005)
M6	$IO + HO_2 \rightarrow HOI + O_2$	1.40×10^{-11}	540	Atkinson et al. (2007)
M7	$IO + NO \rightarrow I + NO_2$	7.15×10^{-12}	300	Atkinson et al. (2007)
M8	$HO + CH_3I \rightarrow H_2O + I\,(CH_2I)$	4.30×10^{-12}	−1120	Atkinson et al. (2008)
M9	$INO + INO \rightarrow I_2 + 2NO$	8.40×10^{-11}	−2620	Atkinson et al. (2007)
M10	$INO_2 + INO_2 \rightarrow I_2 + 2NO_2$	4.70×10^{-12}	−1670	Atkinson et al. (2007)
M11	$I_2 + NO_3 \rightarrow I + INO_3$	1.50×10^{-12}	–	Atkinson et al. (2007)
M12	$INO_3 + I \rightarrow I_2 + NO_3$	9.10×10^{-11}	−146	Kaltsoyannis and Plane (2008)
M13	$I + BrO \rightarrow IO + Br$	1.20×10^{-11}	–	Sander et al. (2011)
M14	$IO + Br \rightarrow I + BrO$	2.70×10^{-11}	–	Bedjanian et al. (1997)
M15	$IO + BrO \rightarrow Br + I + O_2$	3.00×10^{-12}	510	Atkinson et al. (2007)
M16	$IO + BrO \rightarrow Br + OIO$	1.20×10^{-11}	510	Atkinson et al. (2007)
M17	$OIO + OIO \rightarrow I_2O_4$	1.50×10^{-10}	–	Gómez Martín et al. (2007)
M18	$OIO + NO \rightarrow NO_2 + IO$	1.10×10^{-12}	542	Atkinson et al. (2007)
M19	$IO + IO \rightarrow I + OIO$	2.16×10^{-11}	180	Atkinson et al. (2007)
M20	$IO + IO \xrightarrow{M} I_2O_2$	3.24×10^{-11}	180	Atkinson et al. (2007)
M21	$IO + OIO \xrightarrow{M} I_2O_3$	1.50×10^{-10}	–	Gómez Martín et al. (2007)
M22	$I_2O_2 \xrightarrow{M} IO + IO$	1.00×10^{12}	−9770	Ordóñez et al. (2012)
M23	$I_2O_2 \xrightarrow{M} OIO + I$	2.50×10^{14}	−9770	Ordóñez et al. (2012)
M24	$I_2O_4 \xrightarrow{M} 2OIO$	3.80×10^{-2}	–	Kaltsoyannis and Plane (2008)
M25	$INO_2 \xrightarrow{M} I + NO_2$	9.94×10^{17}	−11859	McFiggans et al. (2000)
M26	$INO_3 \xrightarrow{M} IO + NO_2$	2.10×10^{15}	−13670	Kaltsoyannis and Plane (2008)

of formation (Kaltsoyannis and Plane, 2008; Sander, 2015) as shown in Table 2. Fractionation between gas and liquid on ice is considered (Parrella et al., 2012; Stuart and Jacobson, 2003). Aerosol iodine is assumed to have the same dry deposition properties as sulfate aerosol.

2.3 Iodine chemistry scheme

The gas phase iodine chemistry is shown in Tables 3 and 4. We include all iodine reactions presented by recent IUPAC (Atkinson et al., 2007, 2008) and JPL 10-6 (Sander et al., 2011) compilations relevant to the troposphere. Some additional reactions are included based on recent work (Sommariva et al., 2012; von Glasow et al., 2002) as justified in Sect. A1.1. Reactions within aerosol following uptake of species (HI, HOI, INO_2, INO_3) and processing of higher iodine oxides (I_2O_X, $X = 2, 3, 4$) after formation of I_2O_X are not treated explicitly but are parametrized as described in Sect. 2.5.

2.4 Photolysis rates

Photolysis reactions are summarized in Table 5. Photolysis rates are calculated online using the standard FAST-J code implementation in GEOS-Chem (Mao et al., 2010). Cross-sections are processed to the seven wavelength bins used by FAST-J (Bian and Prather, 2002). For most cross-sections JPL 10-6 (Sander et al., 2011) values were used. For I_2O_X ($X = 2, 3, 4$) we assume the same absorption cross-section as INO_3, an approach used previously (Bloss et al., 2010). For most species (I_2, HOI, IO, OIO, INO, INO_2, I_2O_2, CH_3I, CH_2I_2, CH_2IBr, and CH_2ICl) we assume a quantum yield of 1, but for INO_3 we use a quantum yield of 0.21 (Sander et al., 2011).

Table 4. Termolecular iodine reactions. The lower pressure limit rate (k_0) is given by: $A_0 \cdot \exp(\frac{Ea}{RT}) \cdot (\frac{300}{T})^x$. The high-pressure limit is given by k_∞. F_c characterizes the fall-off curve of the reaction as described by Atkinson et al. (2007). Unknown values are represented by a dash and these set to zero in the model, reducing the exponent to 1.

Rxn ID	Reaction	A_0 cm^6 molecules^{-2} s^{-1}	Ea/R K	x	k_∞ cm^3 molecules^{-1} s^{-1}	F_c	Citation
T1	$I + NO + M \rightarrow INO + M$	1.80×10^{-32}	300	1	1.70×10^{-11}	0.60	Atkinson et al. (2007)
T2	$I + NO_2 + M \rightarrow INO_2 + M$	3.00×10^{-31}	300	1	6.60×10^{-11}	0.63	Atkinson et al. (2007)
T3	$IO + NO_2 + M \rightarrow INO_3 + M$	7.70×10^{-31}	–	5	1.60×10^{-11}	0.40	Atkinson et al. (2007)

Table 5. Photolysis reactions of iodine species. For I_2O_X ($X = 2$, 3, 4) the cross-section of INO_3 is used as described in Sect. 2.4.

ID	Reaction	Reference cross-section
J1	$I_2 + h\nu \rightarrow 2I$	Sander et al. (2011)
J2	$HOI + h\nu \rightarrow I + OH$	Sander et al. (2011)
J3	$IO + h\nu \rightarrow I + [O_3]$	Sander et al. (2011)
J4	$OIO + h\nu \rightarrow I + O_2$	Sander et al. (2011)
J5	$INO + h\nu \rightarrow I + NO$	Sander et al. (2011)
J6	$INO_2 + h\nu \rightarrow I + NO_2$	Sander et al. (2011)
J7	$INO_3 + h\nu \rightarrow I + NO_3$	Sander et al. (2011)
J8	$I_2O_2 + h\nu \rightarrow I + OIO$	see caption
J9	$CH_3I + h\nu \rightarrow I + CH_2O_2$	Sander et al. (2011)
J10	$CH_2I_2 + h\nu \rightarrow 2I + (CH_2)$	Sander et al. (2011)
J11	$CH_2ICl + h\nu \rightarrow I + (CH_2Cl)$	Sander et al. (2011)
J12	$CH_2IBr + h\nu \rightarrow I + (CH_2Br)$	Sander et al. (2011)
J20	$I_2O_4 + h\nu \rightarrow 2OIO$	see caption
J21	$I_2O_3 + h\nu \rightarrow OIO + IO$	see caption

2.5 Heterogeneous processes

In line with previous studies (McFiggans et al., 2000), we consider that the uptake of HOI, INO_2, and INO_3 leads to the recycling of iodine back into the gas phase as $1/2I_2$ on sea-salt aerosol alone, whereas irreversible loss via uptake of HI leads to the generation of aerosol phase iodine. Uptake of I_2O_X ($X = 2$, 3, 4) also leads to the generation of aerosol phase iodine (on any aerosol). Heterogeneous uptake rates are computed using the GEOS-Chem standard code (Jacob, 2000) from reactive uptake coefficients (γ). Reactions considered and values of γ used are based on recommendations and previous studies (see Table 6 and Sect. A1.2).

2.6 Model bromine chemistry

The bromine simulation in GEOS-Chem is described in Parrella et al. (2012) and this bromine chemistry is included in the simulations "BROMINE" and "Br+I" in the paper. Parrella et al. (2012) presented a range of comparisons against satellite BrO observations. Although in general the model reproduces many of the features, there is a systematic underestimation of tropospheric BrO. New aircraft observations show that tropospheric BrO (Volkamer et al., 2015; Wang et al., 2015) may be higher than within our simulation. Our simulation also underestimates surface BrO observed in the tropical Atlantic marine boundary layer ($900\,hPa < p$) (~ 2 pmol mol^{-1}, Read et al., 2008) by a ratio of ~ 5 (0.4 pmol mol^{-1}). We consider the uncertainty in BrO concentration on our simulation as a part of our sensitivity study in Sect. 7.

3 Iodine model results and observation comparisons

In this section we describe and evaluate our iodine simulation ("Br+I"), which includes both iodine and bromine chemistry (Sect. 2.6). We initially focus on observational constraints for those iodine compounds that are directly emitted (Sect. 3.1), and then on the only secondary product which has been comprehensively observed (IO) (Sect. 3.2). We then turn to the averaged distribution of modelled iodinated compounds throughout the troposphere (Sect. 4).

3.1 Emitted iodine compounds

Figures 2 and 3 show annually averaged zonal (Fig. 2) and surface concentrations (Fig. 3) of organic and inorganic iodine precursors and their degradation products. These figures clearly illustrate the oceanic nature of iodine source species (CH_3I, CH_2I_2, CH_2ICl, CH_2IBr, HOI, I_2), with the highest concentrations over the tropical ocean. These plots also highlight the contribution of the included terrestrial CH_3I paddy field source (25 %) to global CH_3I concentrations from the Bell et al. (2002) emissions included in Ordóñez et al. (2012).

The emissions used here for organic iodine species have been assessed in Ordóñez et al. (2012). We briefly present here a comparison between observations of CH_3I and CH_2ICl (Fig. 4) made during the UK Combined Airborne Studies in the Tropics (CAST) campaign over the tropical Pacific (Guam) from January and February of 2014. These observations were made by gas chromatography mass spectrometry as described in Andrews et al. (2015), using whole air samples from the Facility Airborne Atmospheric Measurement BAe 146-301 atmospheric research aircraft with techniques described in Andrews et al. (2013). The model shows an ability to capture the trend of decreasing concentration profile with height, but appears to underestimate the CH_3I concentrations (Fig. 4). Concentrations of CH_2ICl ap-

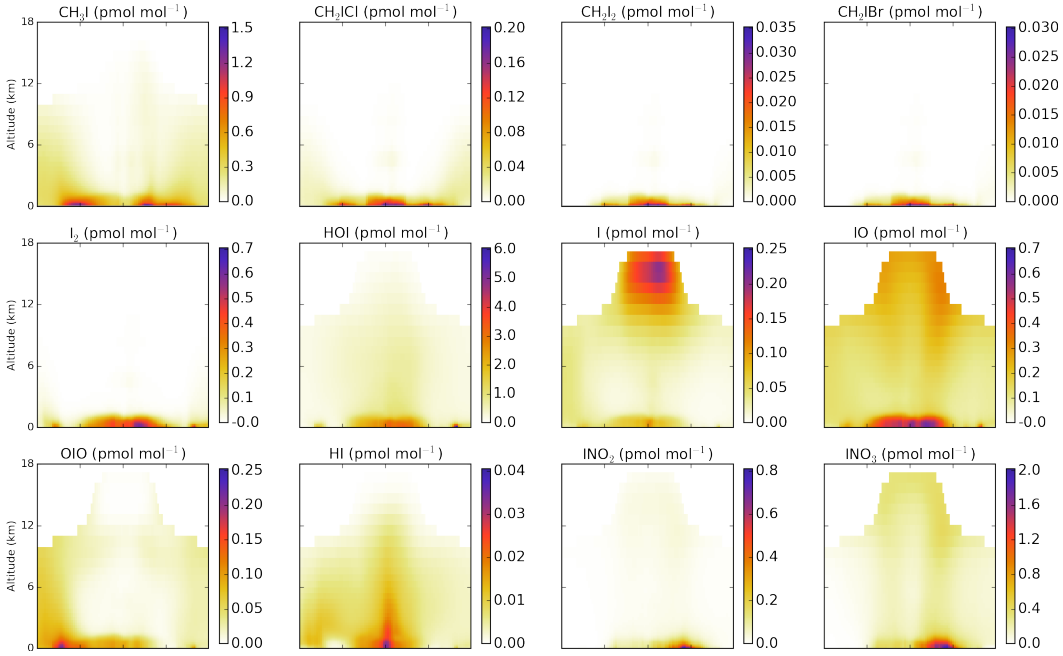

Figure 2. Annual mean zonal tropospheric mixing ratios for precursor and reactive iodine compounds (pmol mol^{-1}) in the simulation with both iodine and bromine chemistry ("Br+I"). No calculations of concentrations are made within the stratosphere and so that region is left blank.

Table 6. Heterogeneous reactions of iodine species. Where measured values have not been reported estimated values are used and no reference is given, further detail on uptake choices is in Sect. A1.2. Asterisked (*) reactions proceed only on sea-salt aerosols.

ID	Reaction	Reactive uptake coefficient (γ)	Reference
K1	HI $\rightarrow$ iodine aerosol	0.10*	Crowley et al. (2010)
K2	$INO_3 \rightarrow 0.5I_2$	0.01*	see caption text
K3	HOI $\rightarrow 0.5I_2$	0.01*	Sander et al. (2011)
K4	$INO_2 \rightarrow 0.5I_2$	0.02*	see caption text
K5	$I_2O_2 \rightarrow$ iodine aerosol	0.02	see caption text
K6	$I_2O_4 \rightarrow$ iodine aerosol	0.02	see caption text
K7	$I_2O_3 \rightarrow$ iodine aerosol	0.02	see caption text

pear to be better simulated in the marine boundary layer (900 hPa $< p$) where measurements are available (Fig. 4). Although not definitive, this brief comparison suggests that the model, if anything, underestimates the concentration of organic iodine.

The first in situ remote open ocean I_2 concentration measurements were made at Cape Verde (Lawler et al., 2014). This data set reported concentrations increasing between dusk and dawn in the range 0.2 to 1.7 pmol mol^{-1} for the two separate measurement campaigns in May 2007 and May 2009 respectively. Our model captures the diurnal variation in I_2 of essentially zero during the day and increasing I_2 concentration during the night, peaking just before dawn, but ranges between 2.5 and 7.5 pmol mol^{-1}. Some component of this overestimate probably relates to the model's iodine heterogenous recycling which assumes 100 % conversion of HOI, INO_3, and INO_2 into $1/2I_2$ rather than ICl and IBr which has been observed in laboratory studies (Braban et al., 2007).

3.2 Iodine oxide (IO) observations

Effectively, the only secondary iodine compound that has been observed and reported is IO. A comparison of a range of surface observations is shown in Fig. 5. Good agreement is seen in the West Pacific (TransBrom, Großmann et al., 2013) and tropical Atlantic at Cape Verde (Mahajan et al., 2010; Read et al., 2008), but the model has a generally high bias compared with other data sets (HALOCast-P, Mahajan et al., 2012; Malasapina, Prados-Roman et al., 2015b, TORERO ship Volkamer et al., 2015).

Biases between the daytime modelled and measured IO at Cape Verde and during the TransBrom cruise biases are

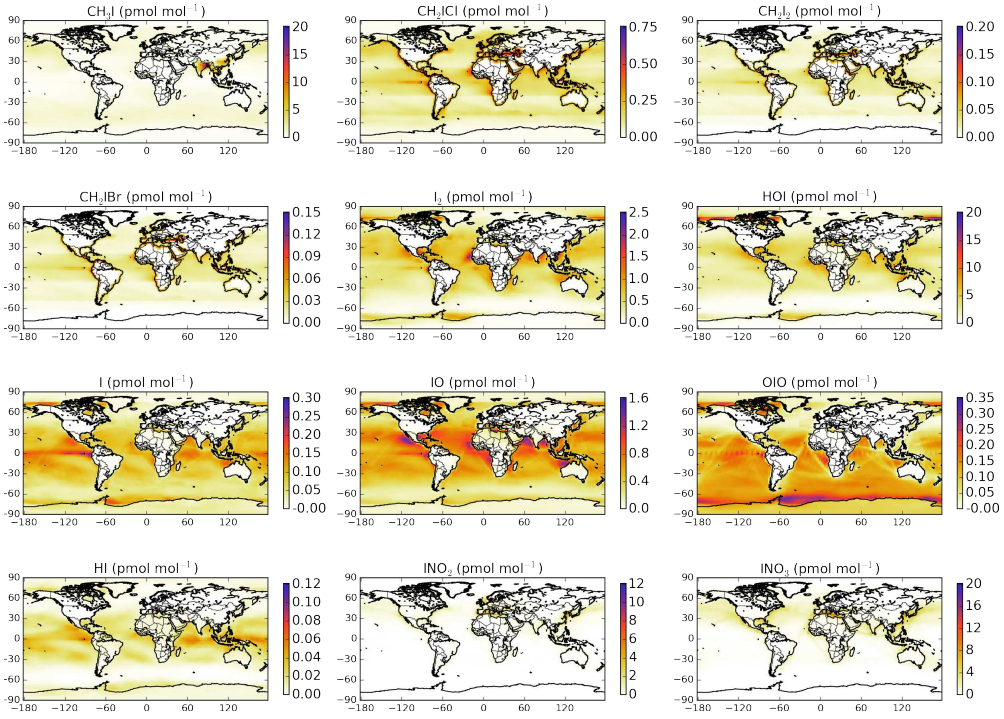

Figure 3. Annual mean surface mixing ratios for precursor and reactive iodine (pmol mol^{-1}) in the simulation with both iodine and bromine chemistry ("Br+I").

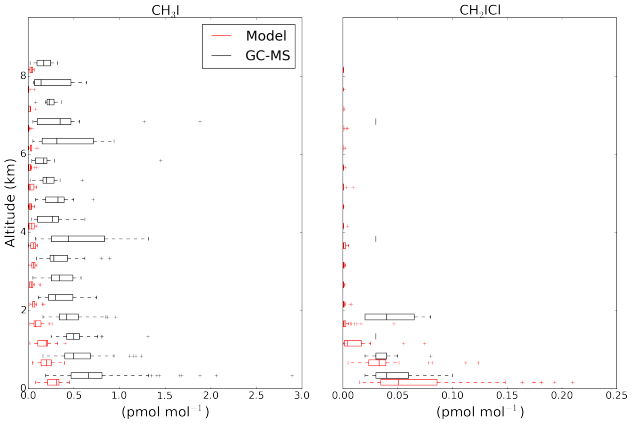

Figure 4. Vertical comparison of observations from the CAST (Combined Airborne Studies in the Tropics) campaign in the mid-Pacific (Guam). The observations are shown in black and simulated values with both iodine and bromine chemistry ("Br+I") in red. Values are considered in 0.5 km bins, with observations and modelled values at the same location and time (as described in Sect. 2) shown side-by-side around the mid-point of each bin. The observations are from the FAAM BAE-146 research aircraft whole air samples analysed by Gas Chromatography–Mass Spectrometry (GC-MS). The box plot extents give the inter-quartile range, with the median shown within the box. The whiskers give the most extreme point within 1.5 times the inter-quartile range.

within ~ 22 and $\sim 16\,\%$ respectively. However, the model overestimates the Malasapina cruise IO concentrations (bias $\sim +50$ to $250\,\%$), TORERO ship observations (bias $+114$–$164\,\%$), and both under- and over- estimates values from the HALOCast-P cruise (bias ~ -0.92 to $280\,\%$). When all observations are latitudinally averaged (onto a 20° grid), an average bias of $\sim +90\,\%$ is found.

In Fig. 6 we show a comparison with recent aircraft IO observations from the TORERO aircraft campaign (Volkamer et al., 2015; Wang et al., 2015), which took place over the eastern Pacific. The model captures the vertical profile of IO but overestimates the observations (average bias of $+82\,\%$ within the binned comparison). Biases in the comparison are greatest (bias $= +125\,\%$) in the marine boundary layer (900 hPa $< p$) and lowest (bias $= +73\,\%$) in the free troposphere (350 hPa $< p <$ 900 hPa). The median bias in the upper troposphere (350 hPa $> p >$ tropopause) is $+95\,\%$.

From these comparisons it is evident that the model has some skill in simulating the average global surface distribution of IO (within a factor of 2) and similar skill at reproducing average vertical profiles. However, there is significant variability between locations, data sets, and measurement groups. Increased global coverage, especially vertically, and inter-comparison of observational techniques are needed to better constrain the IO distribution.

Table 7. Comparison between global tropospheric O_X budgets of simulations "BROMINE", "Br+I", "IODINE", and "NOHAL" are described here. "BROMINE" includes just bromine chemistry, "Br+I" includes both iodine and bromine chemistry, "IODINE" only includes iodine chemistry, and "NOHAL" is simulation without iodine or bromine chemistry. Recent average model values from Young et al. (2013) are also shown. For the IO + BrO halogen crossover reaction we allocate half the O_3 loss to bromine and half to iodine. Values are rounded to the nearest integer value.

Scenario	"NOHAL"	"IODINE"	"BROMINE"	"Br+I"	ACCENT Young et al. (2013)
O_3 burden (Tg)	390	357	367	334	340 ± 40
O_X chemical sources ($Tg\,yr^{-1}$)					
$NO + HO_2$	3667	3680	3512	3529	–
$NO + CH_3O_2$	1332	1383	1269	1307	–
Other O_X sources	502	518	505	521	–
Total chemical O_X sources (PO_X)	5501	5581	5286	5357	5110 ± 606
O_X chemical sinks ($Tg\,yr^{-1}$)					
$O_3 + h\nu + H_2O \rightarrow 2OH + O_2$	2579	2271	2425	2119	–
$O_3 + HO_2 \rightarrow OH + O_2$	1391	1186	1274	1080	–
$O_3 + OH \rightarrow HO_2 + O_2$	687	627	621	560	–
$HOBr + h\nu \rightarrow Br + OH$	–	–	166	143	–
$HOBr + HBr \rightarrow Br_2 + H_2O$ (aq. aerosol)	–	–	8	8	–
$BrO + BrO \rightarrow 2Br + O_2$	–	–	12	10	–
$BrO + BrO \rightarrow Br_2 + O_2$	–	–	3	3	–
$BrO + OH \rightarrow Br + HO_2$	–	–	6	5	–
$IO + BrO \rightarrow Br + I + O_2$	–	–	–	7	–
Other bromine O_X sinks	–	–	1	1	–
Total bromine O_X sinks	–	–	195	178	–
$HOI + h\nu \rightarrow I + OH$	–	639	–	583	–
$HOI \rightarrow 0.5I_2$ (sea-salt aerosol)	–	2	–	2	–
$IO + BrO \rightarrow Br + I + O_2$	–	–	–	7	–
$OIO + h\nu \rightarrow I + O_2$	–	114	–	156	–
Other iodine O_X sinks	–	1	–	1	–
Total iodine O_X sinks	–	756	–	748	–
Other O_X sinks	176	181	172	179	–
Total chem. O_X sinks (LO_X)	4833	5021	4687	4864	4668 ± 727
O_3 $P(O_X)$-$L(O_X)$ ($Tg\,yr^{-1}$)	668	560	599	493	618 ± 251
O_3 Dry deposition ($Tg\,yr^{-1}$)	949	850	886	791	1003 ± 200
O_3 Lifetime (days)	25	22	24	22	22 ± 2
O_3 STE (PO_X-LO_X-Dry dep.) ($Tg\,yr^{-1}$)	281	290	287	298	552 ± 168

4 Modelled distribution of iodinated compounds

We now analyse the modelled distribution of iodinated compounds. We start with the total gas phase inorganic iodine I_Y species ($2I_2 + HOI + IO + OIO + HI + INO + INO_2 + INO_3 + 2I_2O_2 + 2I_2O_3 + 2I_2O_4$) and then move to the distribution of the IO_X (I + IO) family.

4.1 Total inorganic iodine (I_Y)

The modelled iodine system is schematically shown in Fig. 7. Iodine emissions total $3.8\,Tg\,I\,yr^{-1}$ with most of this ($3.2\,Tg\,I\,yr^{-1}$) coming from the inorganic source (84 %). This is comparable to the 83 % calculated by Prados-Roman et al. (2015b) (Ocean only, 60° N–60° S). Most (56 %) of the emissions occur in the Tropics (22° S to 22° N). Our emissions, which include inorganic emissions, compare with reported values of $1.8\,Tg\,I\,yr^{-1}$ (Saiz-Lopez et al., 2012a) and $2.6\,Tg\,I\,yr^{-1}$ (Saiz-Lopez et al., 2014) which also include an inorganic source. Previous studies that did not consider an inorganic iodine source give values of $0.58\,Tg\,I\,yr^{-1}$ (Ordóñez et al., 2012), and $0.65\,Tg\,I\,yr^{-1}$ (Jones et al., 2010), consistent with our organic emissions. HOI represents the single largest source of oceanic iodine (76 %) with averaged oceanic emissions of 1.4×10^8 atoms (I) $cm^{-2}\,s^{-1}$. This value

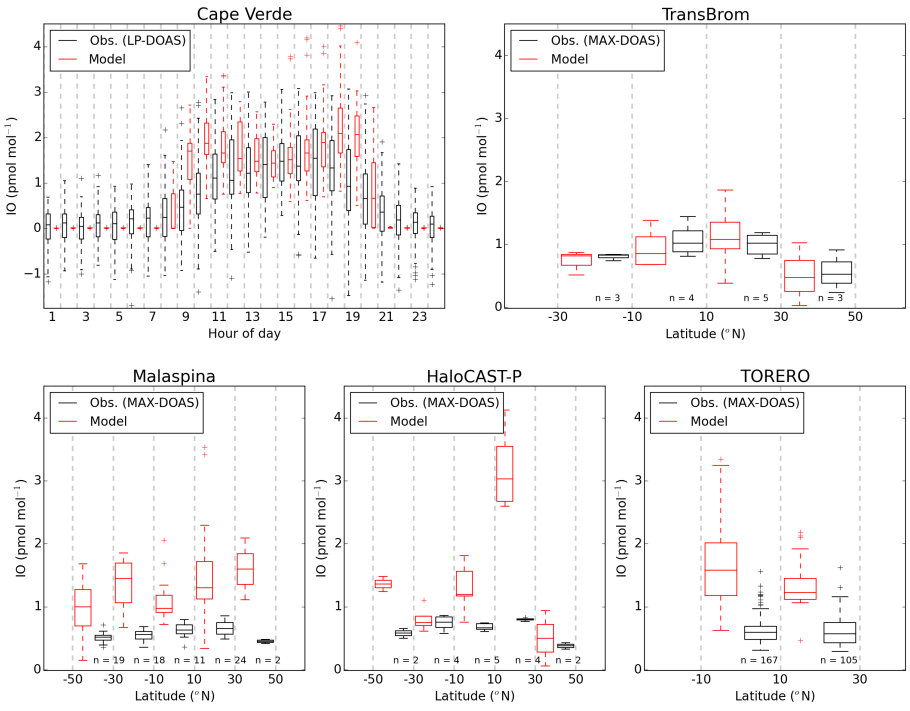

Figure 5. Iodine oxide (IO) surface observations (black) by campaign compared against the simulation with both iodine and bromine chemistry ("Br+I", red). Cape Verde measurements are shown against hour of day and others are shown as a function of latitude. Values are considered in 20° bins, with observations and modelled values at the same location and time (as described in Sect. 2) shown side-by-side around the mid-point of each bin. Extents of bins are highlighted with grey dashed lines. Observations are from Cape Verde (Tropical Atlantic, Mahajan et al., 2010; Read et al., 2008), Transbrom (West Pacific, Großmann et al., 2013), the Malaspina circumnavigation (Prados-Roman et al., 2015b), HaloCAST-P (East Pacific, Mahajan et al., 2012), and TORERO ship (East Pacific, Volkamer et al., 2015). Number of data points within latitudinal bin are shown as "n". The boxplot extents give the inter-quartile range, with the median shown within the box. The whiskers give the most extreme point within 1.5 times the inter-quartile range.

is towards the lower end of flux values required to reproduce IO observations in recent box modelling studies (Großmann et al., 2013; Jones et al., 2010; Mahajan et al., 2009).

Annual mean surface concentrations (Fig. 3) of IO are ubiquitously found over the oceans at ~ 0.25–1 pmol mol^{-1}. Minor species (e.g. HI, OIO) are modelled at greatest mixing ratios over the tropical oceans and towards the poles. Iodine compounds are formed through interacts with NO_X (INO_3/INO_2) peaking in the Northern Hemisphere in polluted oceanic regions. However, due to limited or non-existent measurements of these species in the remote marine boundary layer, these species offer limited ability to constrain the modelled values.

Iodine deposition is predominantly through HOI (51 %). The remainder is mostly through deposition of INO_3 (20 %) and aerosol iodine formed by heterogeneous loss of gaseous iodine (HI, I_2O_X) (24 %). The majority of the deposition sink is back into the ocean (91 %). The global I_Y lifetime is 3.3 days but where depositional scavenging is weakest (upper troposphere, 350 hPa $> p >$ tropopause) this can increase by 2 orders of magnitudes.

Figures 8 and 9 show the average vertical and zonal distribution of iodine compounds through the troposphere. As expected given the surface source, the concentration of iodine drops with altitude. This drop is rapid across the top of the boundary layer. The concentrations of the short-lived source gases – CH_2IX (where $X =$ Cl, Br, I) and I_2 – are negligible outside of the lowest model levels but the concentrations of others (CH_3I and HOI) persist further through the column. For CH_3I this is due to its longer lifetime of ~ 4 days. However, the lifetime of HOI is short (~ 4 min) and its persistence at higher altitudes reflects secondary chemical sources. From the top of the boundary layer to ~ 10 km the I_Y profile is flat due to the rapid convective mixing within the Tropics. However, above this mixing zone the concentrations decrease. The inorganic iodine within the tropical (22° N–22° S) upper troposphere (> 10 km) is approximately equally sourced from upwards I_Y flux (6.6 Gg yr^{-1}) and organic iodine photolysis (7.9 Gg yr^{-1}), overwhelmingly of CH_3I. Overall, atmospheric iodine is dominated by three IOy species (HOI, IO, and INO_3) with HOI representing the greatest fraction (~ 70 %) in the free troposphere (350 hPa $< p <$ 900 hPa).

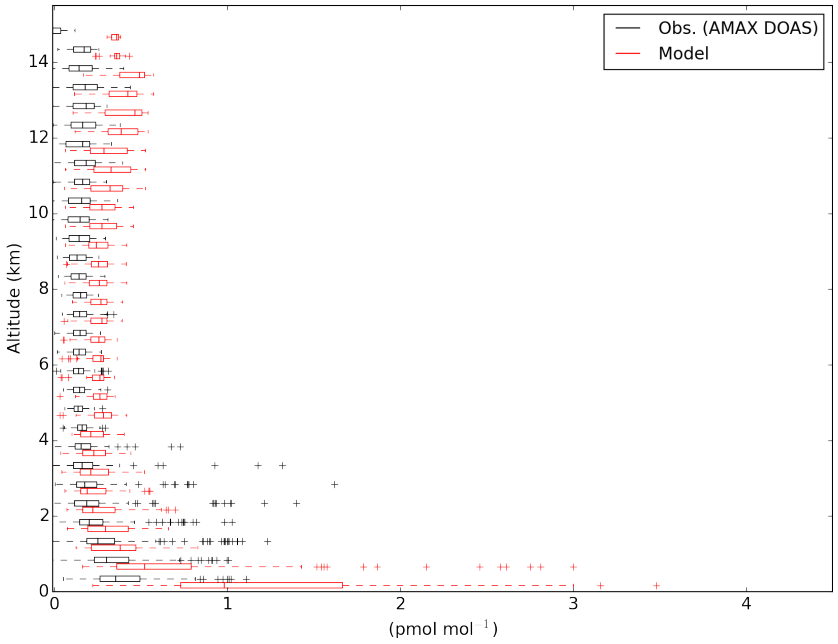

Figure 6. Vertical comparison of the simulation with both iodine and bromine chemistry ("Br+I") and measured iodine oxide (IO) during TORERO aircraft campaign (Volkamer et al., 2015; Wang et al., 2015). Model and observations are in red and black respectively. Values are considered in 0.5 km bins, with observations and modelled values at the same location and time (as described in Sect. 2) shown side-by-side around the mid-point of each bin. Measurements were taken aboard the NSF/NCAR GV research aircraft by the University of Colorado airborne Multi-Axis DOAS instrument (CU AMAX-DOAS) in the eastern Pacific in January and February 2012 (Volkamer et al., 2015; Wang et al., 2015) . The boxplot extents give the inter-quartile range, with the median shown within the box. The whiskers give the most extreme point within 1.5 times the inter-quartile range.

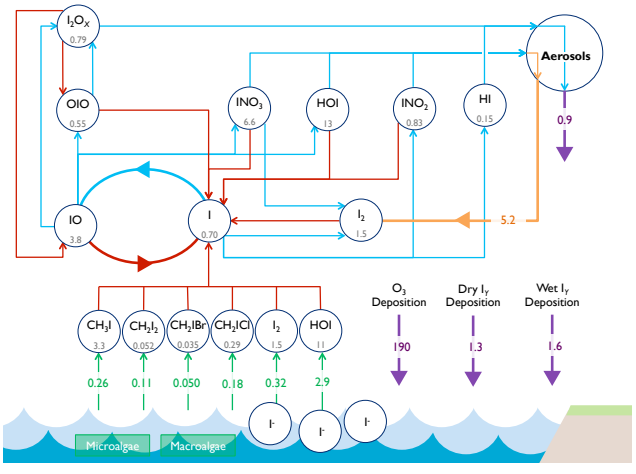

Figure 7. Schematic representation of implemented iodine chemistry in the simulation with both iodine and bromine chemistry ("Br+I"). Average global annual mean burdens (Gg I) are shown below key I_Y species, with fluxes (Tg I yr^{-1}) shown on arrows. Red lines, photolysis; blue lines, chemical pathways; green lines, emission source; orange lines, heterogeneous pathway; purple lines, depositional pathway. This equates to a total iodine source and sink of 3.8 Tg I yr^{-1}. O_3 deposition in Tg is also shown to illustrate the driving force behind the inorganic emissions.

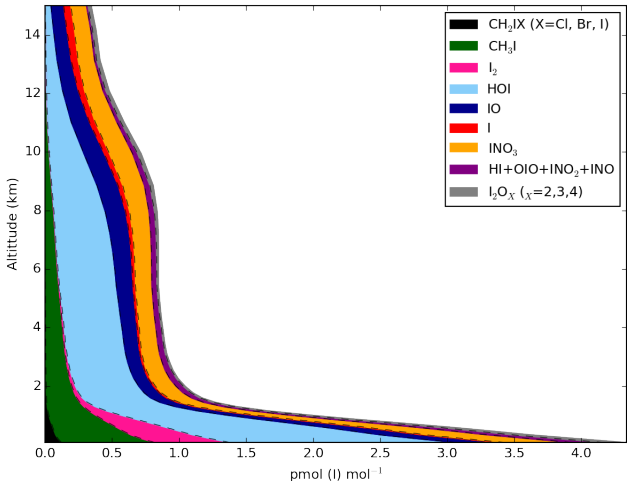

Figure 8. Global annual mean gas-phase iodine speciation with altitude in the simulation with both iodine and bromine chemistry ("Br+I"). Mixing ratios are shown in pmol mol^{-1}, with higher iodine oxides (I_2O_X ($X = 2$, 3, 4)) and di-halogenated organics (CH_2IX ($X =$ Cl, Br, I)) grouped.

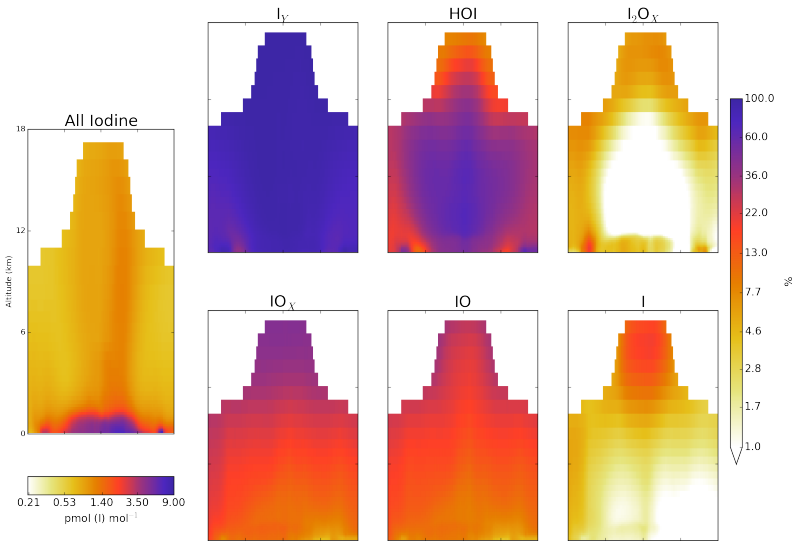

Figure 9. Zonal breakdown of global annual mean iodine speciation by family in the "Br+I" simulation. First panel shows total gas phase iodine concentration and the following panels show percentage of different compounds to this. Total gas phase iodine ("All Iodine") = $CH_3I + 2CH_2I_2 + CH_2IBr + CH_2ICl + 2I_2 + HOI + IO + OIO + HI + INO_2 + INO_3 + 2I_2O_2 + 2I_2O_3 + 2I_2O_4 + I + INO$; $I_Y = 2I_2 + HOI + IO + OIO + HI + INO + INO_2 + INO_3 + 2I_2O_2 + 2I_2O_3 + 2I_2O_4$; $IO_X = I + IO$.

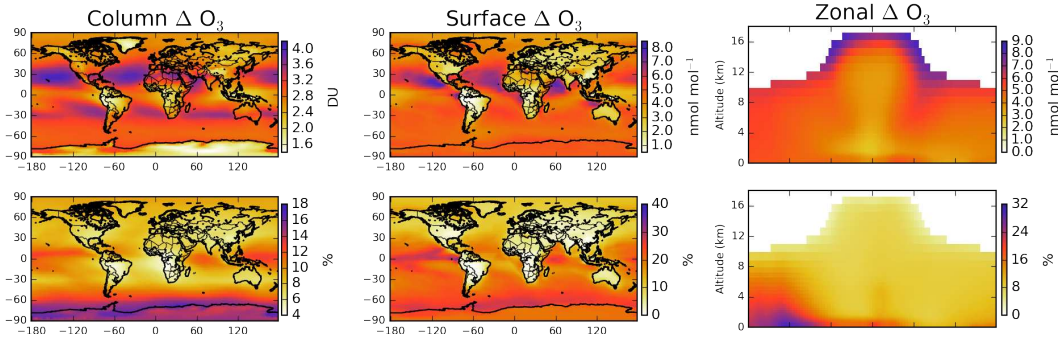

Figure 10. Decreases in annual mean tropospheric column, surface, and zonal O_3 with inclusion of iodine ("Br+I"–"BROMINE") chemistry are shown on left, middle, and right panels respectively. Upper panels show changes in Dobson units or nmol mol^{-1} and lower panels show changes in percentage terms.

4.2 The iodine oxide family: IO_X (I + IO)

Globally, IO_X production is dominated by inorganic iodine I_Y photolysis (HOI, 76 %; OIO, 11 %). The major loss route for IO_X is HOI production through IO reaction with HO_2 (77 %), with additional loss routes through self-reaction, reaction with NO_X, and BrO contributing 10, 7.7, and 4.6 % respectively.

The global average IO_X lifetime with respect to chemical loss is $\sim$ 1 min, but increases within the tropical upper troposphere (350 hPa $> p >$ tropopause) (up to nine times) and beyond latitudes of 80° N and S (up to four times) due to colder temperatures. The major IO formation route (I + O_3) slows in these regions due to colder temperatures. This moves the partitioning of IO_X from IO to I. As the IO_X loss routes proceed predominantly through IO, the overall IO_X lifetime increases. This causes an increase in the annually averaged I to IO ratio which peaks with a ratio of 0.7–1.4 within the tropical upper troposphere (350 hPa $> p >$ tropopause). This is at the lower end of the daytime range of 1–4 previously calculated (Saiz-Lopez et al., 2014). As described in Sect. 4.1, the I_Y (and thus the IO_X) in this region is approximately evenly sourced from photolysis of transported organic iodine species and direct transport of I_Y.

5 Impact of iodine on O_3 and OH

O_3 and OH are two key parameters for climate and air quality. Previous studies (Bloss et al., 2005b; Saiz-Lopez et al., 2008, 2012a) have identified significant impacts of iodine on these compounds. Here we compare our model predictions

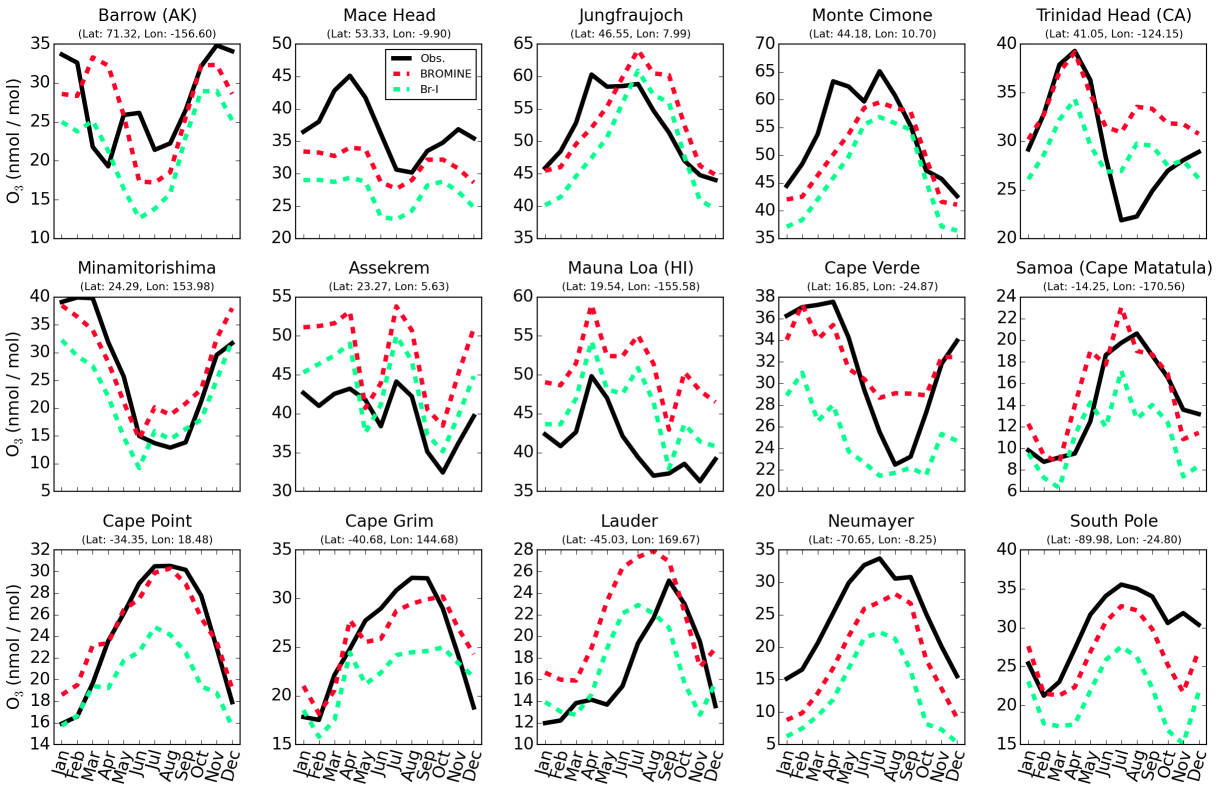

Figure 11. Seasonal cycle of near-surface O_3 at a range of Global Atmospheric Watch (GAW) sites (Sofen and Evans, 2015). Observational data shown are a 6-year monthly average (2006–2012). Model data are for 2005. Data are from GAW compile and processed as described in Sofen and Evans (2015). Red indicates standard GEOS-Chem (v9-2) including bromine chemistry ("BROMINE") and green with inclusion of iodine chemistry ("Br+I").

to available observational constraints and then diagnose the model change.

5.1 Impact on O_3

On inclusion of iodine, the calculated global tropospheric O_3 burden drops from 367 to 334 Tg (9.0 %). Figure 10 shows the annual average tropospheric column, surface, and zonal change in O_3. On average the O_3 burdens in the marine boundary layer (900 hPa $< p$) decreased by 19.5 %, by 9.8 % in the free troposphere (350 hPa $< p <$ 900 hPa), and 6.2 % in the upper troposphere (350 hPa $> p >$ tropopause). The decrease is greater in the Southern Hemisphere (9.5 %), than the Northern Hemisphere (8.5 %).

Surface (lowermost model level) O_3 shows an average decrease of 3.5 nmol mol^{-1} globally, with large spatial variability (Fig. 11) with a greater decrease over the oceans (21 %) than the land (7.3 %). Comparing against the Global Atmospheric Watch (GAW, Sofen and Evans, 2015) surface O_3 observations (Fig. 11), there is no obvious decrease in the ability of the model to capture seasonality in surface O_3 although there is systematic decrease in O_3 concentration with the inclusion of iodine.

Figure 12 shows a comparison between a selection of annually averaged O_3 sonde profiles for the same year (2005, World Ozone and Ultraviolet Data Centre WOUDC, 2014) and our model simulation with and without iodine. A decrease in O_3 concentration is evident throughout the troposphere (average of 3.1 nmol mol^{-1}). As with comparison of surface observations (Fig. 12), no clear decline in model skill at capturing annual sonde profiles is apparent on inclusion of iodine, with some locations improving and others degrading. An exception to this is O_3 observations south of 60° S at the surface where biases are increased and in the tropical free troposphere (350 hPa $< p <$ 900 hPa) where model O_3 biases are decreased.

5.2 O_3 budget

We diagnose the impact of iodine on O_3 by calculating the model's tropospheric odd oxygen (O_X) budget in Table 7. Here we define O_X as defined in footnote 1.

Iodine provides a global tropospheric O_X loss of 748 Tg yr^{-1} (15 % of the total). This is significantly larger than the 178 Tg yr^{-1} from bromine chemistry and is comparable to the sink from the $O_3 + OH$ reaction. Overwhelmingly this loss is from the photolysis of HOI after its produc-

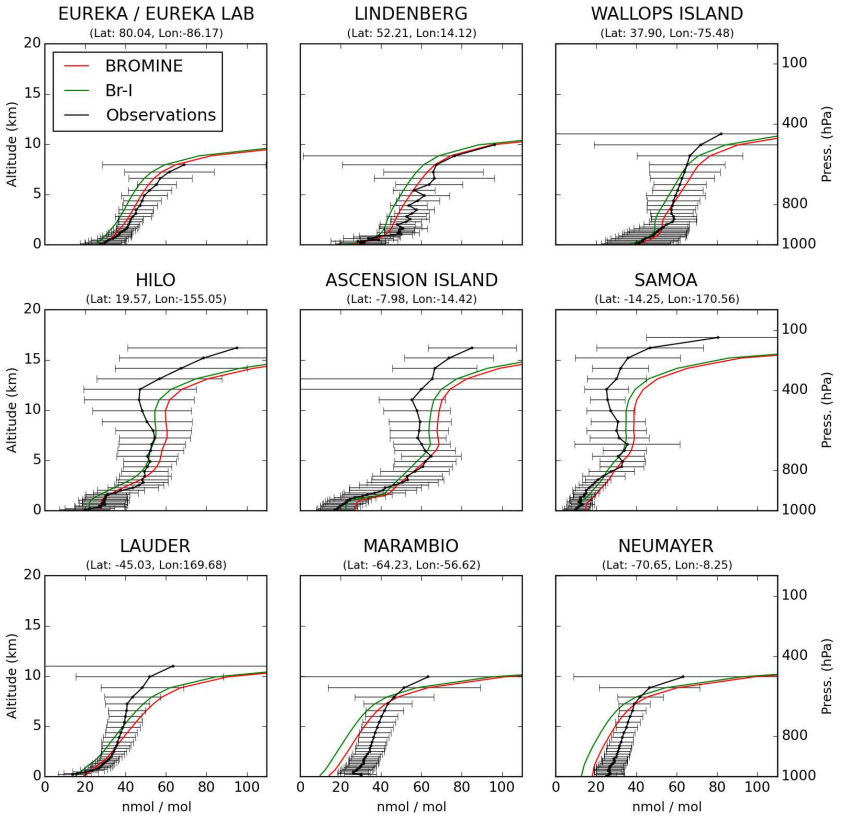

Figure 12. Comparison between annual modelled O_3 profiles and sonde data (2005, WOUDC, 2014). Profiles shown are the annual mean of available observations from World Ozone and Ultraviolet Radiation Data Centre WOUDC (2014) and model data for 2005 at given locations. Red indicates standard GEOS-Chem (v9-2) including bromine chemistry ("BROMINE") and green with inclusion of iodine chemistry ("Br+I"). Observations (in black) show mean concentrations with upper and lower quartiles given by whiskers.

tion from the reaction of IO with HO_2. The O_3 production term increases slightly ($\sim 1\,\%$) with the inclusion of iodine reflecting small changes in the total reactive nitrogen partitioning.

Iodine-induced O_3 loss within the marine (land mask applied and between 50° N–50° S) troposphere of $\sim 540\,\mathrm{Tg\,yr^{-1}}$ is comparable to the previously reported values of Saiz-Lopez et al. (2014) when I_2O_X ($X = 2, 3, 4$) photolysis is included ($\sim 500\,\mathrm{Tg\,yr^{-1}}$).

Figure 13 shows the relative importance of different O_X sinks in the vertical. The "classical" O_3 loss routes ($h\nu + H_2O$, HO_X) dominate; however, within the boundary layer and the upper troposphere (350 hPa $> p >$ tropopause), iodine represents 33 and 26 % of the total loss, respectively. The loss within the marine boundary layer (900 hPa $< p$) is comparable to the 28 % reported in Prados-Roman et al. (2015a). This decreases rapidly with increasing altitude within the lower troposphere to values closer to 10 %, reflecting the lower of IO concentrations (see Figs. 8 and 9). In the upper troposphere, higher IO_X and BrO_X concentrations lead to increased loss of O_3.

Figure 14 shows the zonal variation in the different O_X destruction terms (in terms of the O_X lifetime). It is evi-

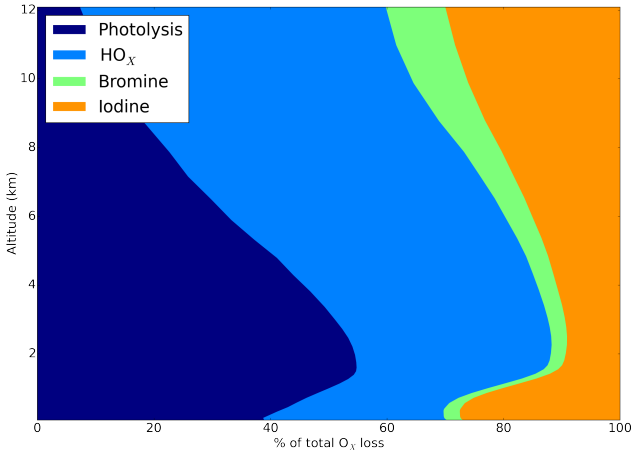

Figure 13. Vertical profile of simulated fractional global annual mean O_X loss by route in the "Br+I" simulation. O_X definition is given in footnote 1. Photolysis represents loss of O_X due to O_3 photolysis in the presence of water vapour. HO_X loss includes routes via minor NO_X channels. The magnitude of the bromine route is probably underestimated, as discussed in Sect. 2.6.

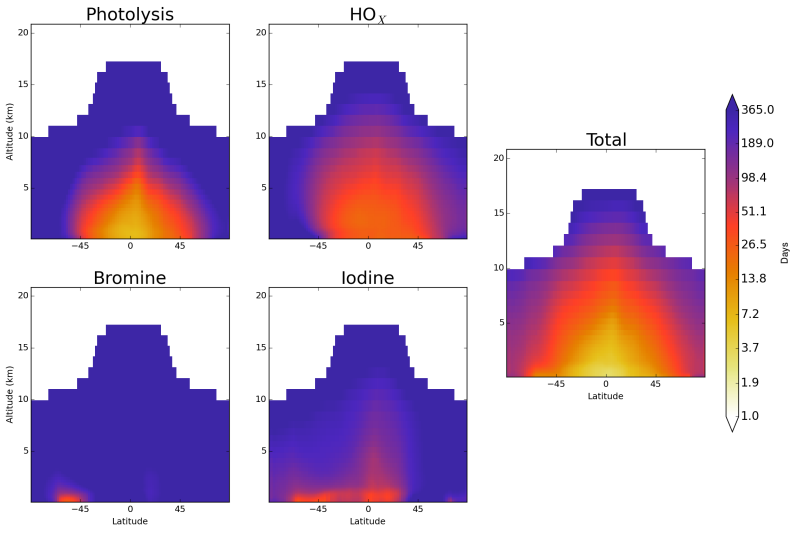

Figure 14. Global annual O_3 mean zonal chemical lifetime for different O_X loss routes (Photolysis, HO_X, Iodine, Bromine, and Total) in the "Br+I" simulation. Values are shown on a log scale.

dent that, in the model, iodine destruction is more spatially prevalent than bromine destruction, which is confined predominantly to the Southern Ocean. The impact of iodine is hemispherically asymmetric, reflecting the higher NO_X in the Northern Hemisphere, higher BrO concentrations in the southern oceans, and the larger ocean area in the Southern Hemisphere increasing emissions. Convective transport in the Tropics rapidly lifts iodine species into the free troposphere (350 hPa $< p <$ 900 hPa) where they can destroy O_3.

5.3 Impact on OH

Previous box model studies which investigated the impact of iodine on OH concentration in the Antarctic (Saiz-Lopez et al., 2008), mid-latitude coastal (Bloss et al., 2005a), tropical marine regions (Mahajan et al., 2010), and the free troposphere (Wang et al., 2015) found increases in the OH concentration due to IO enhancing conversion of HO_2 to OH. However, we find that the inclusion of iodine in the model has little impact on the global mean OH concentrations with it slightly increasing from 12.2 to 12.5×10^5 molecules cm^{-3} (1.8 %). This small increase is surprising given the 12 % reduction in the primary source ($O_3 + H_2O + h\nu$) due to lower O_3 concentrations. However, this is more than compensated for by an increase in the rate of conversion of HO_2 to OH by IO. Previous studies using constrained box models (Bloss et al., 2005a; Saiz-Lopez et al., 2008) could not consider this impact on the primary production of OH and it appears from our simulation that the overall impact is lower than previously thought.

6 Combined impact of bromine and iodine

The importance of halogen cross-over reactions (BrO + IO) for O_3 loss has been previously highlighted and found to be required to replicate observed diurnal surface O_3 loss in the marine boundary layer (Read et al., 2008). To explore these interactions a further two runs were performed, one simulation with iodine but without bromine ("IODINE") and one without any halogens ("NOHAL").

As shown in Table 7, the global tropospheric burdens of O_3 are 390, 367 (reduction of 5.9 %), 357 (8.5 %) and 334 Tg (14 %) for the simulations without halogens ("NOHAL"), with just bromine ("BROMINE"), with just iodine ("IODINE"), and with both iodine and bromine chemistry ("Br+I") respectively. The sum of the changes in O_3 burden for the runs considering halogens individually is slightly lower (0.1 %) than when considered simultaneously.

Figure 15 shows the combined daily surface loss rate of O_3 driven by bromine and iodine (upper panel). This correlates with IO concentrations (Fig. 3) reflecting iodine's role in marine boundary layer O_3 destruction. Figure 15 also shows modelled and observed fractional diurnal fractional O_3 change at Cape Verde in the remote marine boundary layer (lower panel). For this comparison, observations (2006 to 2012, Sofen and Evans, 2015) and model data were first processed to average fractional diurnal change by averaging the values by hour of day, then subtracting the maximum average value of the diurnal. This fractional change was then divided by the average maximum value and multiplied by 100 to give a percentage to allow comparison between simulation runs with different O_3 concentrations.

The simulation's fidelity increases significantly with the inclusion of iodine (Fig. 15) but there is little impact from bromine. Whereas modelled IO concentrations at Cape Verde

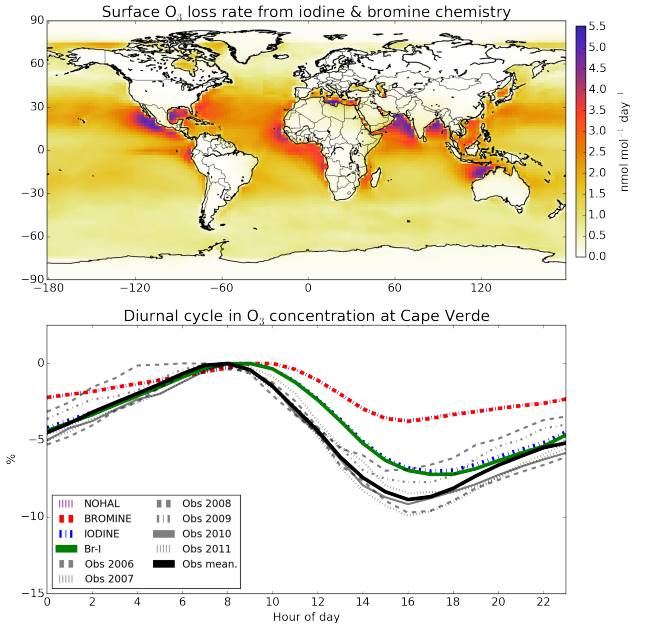

Figure 15. Global annual mean surface O_3 loss (nmol mol^{-1} day^{-1}) in the "Br+I" simulation from both bromine and iodine (top). Comparison between modelled and observed fractional diurnal O_3 cycles at the Cape Verde Observatory for "NOHAL", "BROMINE", "IODINE", and "Br+I" simulations (bottom). The calculation is described in Sect. 6. Diurnal changes are averaged over the whole data set. Lines are black, purple, red, blue, and green for mean of observations, "NOHAL", "BROMINE", "IODINE", and "Br+I" respectively. Individual years of observational data are shown in grey.

show agreement with observations (Fig. 5), BrO concentrations (~ 0.4 pmol mol^{-1}) are significantly lower than reported (~ 2 pmol mol^{-1}, Read et al., 2008). This underestimate of BrO in the model is a systemic problem (see Sect. 2.6) and so model estimates of the impact of Br on atmospheric composition described here are probably an underestimate.

Global mean tropospheric concentrations of OH are 12.80, 12.24, 13.02, and 12.47×10^5 molecules cm^{-3} for the simulations without halogens ("NOHAL"), with just bromine ("BROMINE"), with just iodine ("IODINE"), and with both iodine and bromine chemistry ("Br+I") respectively. OH shows a differing response to bromine and iodine chemistry. As discussed in Sect. 5.3, inclusion of iodine leads to a small increase in OH concentrations. When solely iodine is considered, OH concentrations increase by 1.8 % compared to when no halogens are included. Bromine chemistry leads to a reduction in OH (4.3 %), as reported previously (Parrella et al., 2012), due to enhanced production by HOBr photolysis not compensating for a decrease in the primary OH source ($O_3 + H_2O + h\nu$) from a reduced O_3 burden. The net impact overall on inclusion of halogens is a global reduction in OH (2.6 %).

In our simulations, the global impact of Br and I chemistry are essentially additive with apparently limited impact from the cross-reactions. The global impact of iodine appears significantly larger than that of bromine – however, given that the model underestimates the concentrations of Br compounds this should be subject to future study.

7 Sensitivity studies

As discussed in the Introduction, a range of uncertainties exist in our understanding of tropospheric iodine. We perform sensitivity analysis on some of these parameters using the $4° \times 5°$ version of the model. We chose to analyse the sensitivity to inclusion of inorganic iodine emissions, heterogeneous loss and cycling, photolysis rates, and ocean surface iodide. Values are quoted as a percentage change from the "Br+I" simulation described in Sects. 2–5. Figure 17 summarizes the fractional impact of these experiments on the globally averaged vertical distribution of I_Y, O_3, and vertical profile comparison of observations of IO from the TORERO aircraft campaign (Volkamer et al., 2015; Wang et al., 2015). Additional information is listed in Table A1 in Appendix A.

7.1 Just organic iodine

Until recently many studies solely considered organic iodine (Jones et al., 2010; Ordóñez et al., 2012) emissions. As discussed in Sect. 3.1, our simulation uses the Carpenter et al. (2013) inorganic emission parametrization as well as organic iodine emissions from Ordóñez et al. (2012). When we just consider organic iodine emissions ("Just org. I") we find that global I_Y burdens decrease (65 %), and mean surface marine boundary layer (900 hPa $< p$) IO decreases (83 %). The median bias against TORERO aircraft IO observations decreases by 68 % to become a negative bias of -25 %. The decreased I_Y leads to the mean global OH decreasing by 0.64 % and global tropospheric O_3 increasing by 5.5 %.

7.2 Heterogeneous uptake and cycling

There are limited experimental data for the reaction probability (γ) for iodine species on aerosol. Our base case scheme follows the literature precedent (McFiggans et al., 2000) and assumes a heterogeneous recycling of unity (e.g. HOI $\rightarrow 1/2I_2$) on sea salt which is not limited by aerosol acidity. However, the acidity of aerosol may limit iodine cycling as not all sea-salt aerosols are acidic (Alexander, 2005) and other aerosols may irreversibly uptake iodine. Detail on the γ chosen is in Appendix A (Sect. A1.2). To explore these uncertainties four simulations were run: (1) with the γ values that lead to I_2 release doubled ("het. cycle × 2"), (2) with the γ values halved ("het. cycle/2"), (3) with all uptake reactions leading to a net loss of iodine ("No het. cycle"), and (4) a run where sulfate aerosol leads to a sink for iodine with the same γ values as for sea salt ("Sulfate uptake").

Increasing the heterogeneous cycling ("het. cycle × 2") converts more HOI (the dominant I_Y species) into I_2, thus reducing the rate of HOI deposition. The global I_Y burden increases by 6 %, mean surface marine boundary layer (900 hPa < p) IO concentration increases by 2 %, and the median bias with respect to the TORERO aircraft IO observations increases by 26 to 100 % (Fig. 17). Decreasing the heterogeneous cycling ("het. cycle/2") has the opposite impact of roughly the same magnitude – global average I_Y burden decreases (4.3 %), average surface marine boundary layer IO decreases (1.8 %) and the median bias with respect to the TORERO aircraft IO observations decreases (18 %) to 66 %.

The impacts of these changes is small overall. Increased iodine cycling leads to a decrease in the tropospheric O_3 burden of 0.69 % and global mean OH increases by 0.05 %, whereas decreased cycling leads to the tropospheric O_3 burden increasing by 0.56 % and OH decreasing by 0.09 %.

By removing the release of I_2 to the gas-phase following uptake of iodine ("no het. cycle") or by considering irreversible iodine loss to sulfate aerosol ("Sulfate uptake") the global I_Y burdens decrease significantly by 47 and 48 %, respectively. Surface marine boundary layer (900 hPa < p) IO concentration decreases by 48 and 22 %. The median bias with respect to the TORERO aircraft IO observations decreases in the case of "no het. cycle" (84 %) to 13 % and decreases in "Sulfate uptake" (92 %) to −6.7 %. The "Sulfate uptake" scenario shifts the median bias with the TORERO aircraft IO observations to be negative, instead of positive (+80 % for "Br+I" at 4° × 5°).

This large decrease in I_Y reduces the potency of iodine chemistry. The reductions in the tropospheric O_3 burdens (4.1 and 4.5 % for "no het. cycle" and "Sulfate uptake") are comparable to the simulation where only organic iodine sources are considered (5.5 %, "Just I Org."). Global mean OH decreases slightly by 0.54 and 0.87 % under these two scenarios. These two sensitivity runs represent large perturbations to the iodine system, highlighting the importance and uncertainties in heterogeneous chemistry.

7.3 Uncertainties in photolysis parameters

Absorption cross-sections and quantum yields for iodine species are few and their temperature dependencies are not known. Notably, the absorption cross-sections for the higher iodine oxides (I_2O_2, I_2O_3, I_2O_4) are highly uncertain (Bloss et al., 2001; Gómez Martín et al., 2005; Spietz et al., 2005) and we use the INO_3 spectrum in our simulation. This uncertainty was tested in three simulations: (1) absorption cross-sections were doubled ("I_2O_X X-sections × 2"), (2) tentative literature assignments of spectra were used for I_2O_3 and I_2O_2 (Bloss et al., 2001; Gómez Martín et al., 2005; Spietz et al., 2005), with I_2O_2 used for I_2O_4 ("I_2O_X exp. X-sections"), (3) and finally no I_2O_X photolysis at all was considered ("No I_2O_X photolysis").

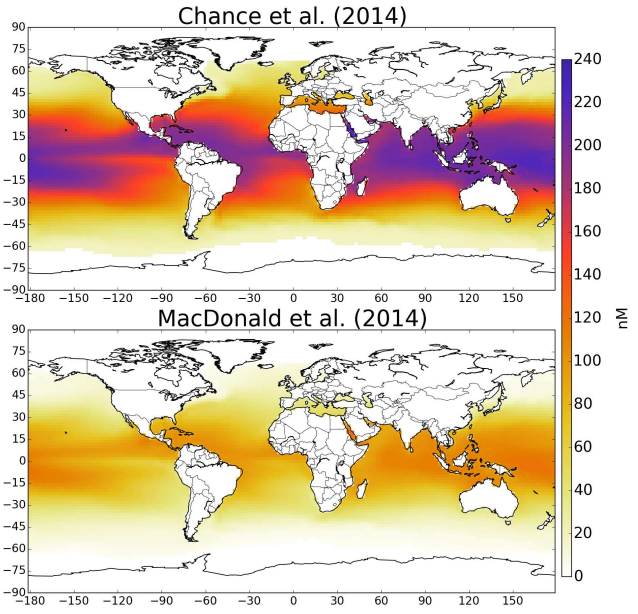

Figure 16. Calculated annual mean ocean surface iodide concentrations (I^-) in nM. Values are calculated from the highest correlation relationship (square) presented in Table 2 of Chance et al. (2014) (top panel) and from the Arrhenius relationship from Eq. (1) in MacDonald et al. (2014) (bottom panel). The Chance et al. (2014) parametrization is used as the standard in the work with the MacDonald et al. (2014) used as the "Ocean iodide" sensitivity simulation in Sect. 7.

Sensitivity runs "I_2O_X X-sections × 2" and "I_2O_X exp. X-sections" increase photolysis rates, therefore resulting in an increase in the I_Y lifetime of 5.3 and 8.3 % and the I_Y burdens by 3.1 and 4.8 % respectively. The average surface marine boundary layer (900 hPa < p) IO concentration responds by increasing by 4.3 and 6.7 % for "I_2O_X X-sections × 2" and "I_2O_X exp. X-sections" respectively. Both these simulations increase median bias with TORERO aircraft IO observations by 4.8 to 84 % and 7.6 to 86 %, respectively. The impacts on O_3 burden are small with a decrease of 0.4 and 0.6 % for "I_2O_X X-sections × 2" and "I_2O_X exp. X-sections" respectively. Global mean OH concentrations increase by 0.05 and 0.09 % respectively.

The removal of I_2O_X ($X = 2, 3, 4$) photolysis reduces the global tropospheric I_Y burden (35 %), reduces surface marine boundary layer (900 hPa < p) IO (40 %), increases tropospheric O_3 burden (5.1 %) and decreases global mean OH (0.9 %) with respect to "Br+I". The median bias with respect to the TORERO aircraft IO observations becomes negative and decreases by 81 to −16 %, illustrating a large change in the simulated IO profile by removing the I_2O_X photolysis (Fig. 17). This was also noted by Prados-Roman et al. (2015b) with respect to surface observations.

Our "No I_2O_X photolysis" simulation is akin to the "base" simulation of Saiz-Lopez et al. (2014). This was presented

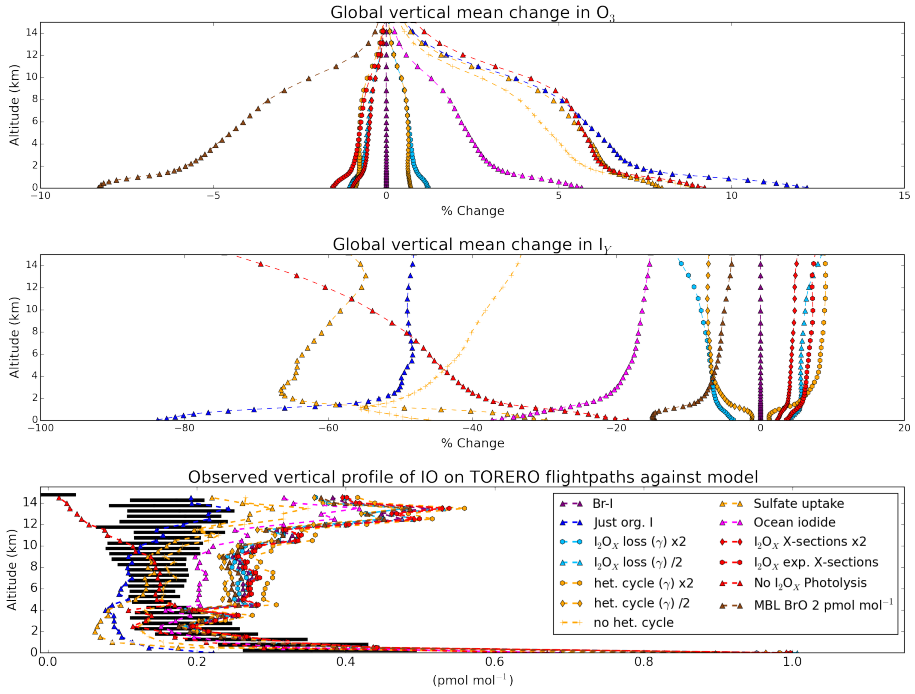

Figure 17. Sensitivity impacts. Upper and middle panels show global mean vertical percentage changes in concentrations of O_3 and I_Y. Lower panel gives vertically averaged iodine oxide (IO) mixing ratios (pmol mol^{-1}) calculated along the TORERO aircraft (Volkamer et al., 2015; Wang et al., 2015) flight paths. The legend (bottom) is shared by all plots. The boxplot of IO observations (black) represents the quartiles of the data, with the median shown within the box.

as a lower bound for iodine chemistry. Their "JI$_X$O$_Y$" simulation, is akin to our "Br+I". Saiz-Lopez et al. (2014) find a decrease in marine tropospheric O_3 column burden of 3.0 and 6.1 % compared to a simulation with no iodine chemistry for their "base" and "JI$_X$O$_Y$" simulations respectively. Considering the same domain, our comparable simulations show values of 4.0 to 8.7 %.

7.4 Marine boundary layer BrO concentration

As discussed in the Introduction and Sect. 6, bromine and iodine chemistry are potentially coupled. GEOS-Chem underestimates BrO (Parrella et al., 2012), with for example, our simulation underestimating the BrO concentrations at Cape Verde (Read et al., 2008) (~ 2 pmol mol^{-1}) by a factor of around 5.

To test the sensitivity of the model to BrO concentrations, a simulation with BrO concentration fixed at 2 pmol mol^{-1} in the daytime marine boundary layer was run ("MBL BrO 2 pmol mol^{-1}"). Increased BrO leads to increased OIO concentrations (BrO+IO $\rightarrow$ OIO+Br), which leads to increased higher oxide production which in turn increases I_Y loss and decreases I_Y burden (10 %). The median bias in vertical comparisons with TORERO aircraft IO observations decreases by 12 to 71 %. Although the overall tropospheric O_3 burden decreases by 3.7 %, the average O_3 change at the surface is larger and shows a decrease of 88 % (Fig. 17) which is the largest decrease in O_3 found within these sensitivity simulations.

7.5 Ocean surface iodide (I^-) concentration

Chance et al. (2014) compiled the available ocean surface iodide (I^-) observations and investigated correlations with various environmental parameters. They found that ocean surface iodide correlated most strongly with the square of sea surface temperature, as used in this work. However, MacDonald et al. (2014), using a sub-set of the Chance et al. (2014) data, found that an Arrhenius parametrization gave best agreement. Figure 16 shows annual averaged ocean surface iodide generated from both parametrizations. The sea surface temperatures are taken from the annual average GEOS field used in GEOS-Chem. The area weighted mean concentrations are 37.6 and 80.8 nM for MacDonald et al. (2014) and Chance et al. (2014), respectively. Both approaches reproduce the latitudinal gradient observed in Fig. 1 of Chance et al. (2014); however, large differences are apparent in magnitude. The data set reported in Chance et al. (2014) has a median value of 77 nM and interquartile range of 28–140 nM.

Inclusion of the MacDonald et al. (2014) iodide parametrization ("Ocean Iodide") reduces the inorganic iodine flux by 51 % to 1.9 Tg, which in turn decreases the global tropospheric iodine I_Y burden (23 %) and surface IO

concentrations (34 %). The median bias in comparison with TORERO vertical profiles decreases by 47 to 42 %. Tropospheric O_3 burden increases by 2.1 % and global mean OH increases by 0.17 % with respect to "Br+I".

7.6 Higher-oxide lifetime

Within the model we have considered the uptake of the I_2O_X ($X = 2, 3, 4$) to aerosol as an irreversible loss of iodine, with the same reactive probability (γ) as INO_2 (0.02). We assess our sensitivity to this assumption by running simulations doubling ("I_2O_X $(\gamma) \times 2$") and halving this value ("I_2O_X $(\gamma)/2$").

The effect of doubling γ leads to decreasing global tropospheric I_Y burden (5.1 %), decreasing surface marine boundary layer (900 hPa $< p$) IO (4.6 %), and decreases the median bias in vertical comparisons with TORERO aircraft IO (6.9 %) to 75 %. This leads to a slightly increased global tropospheric O_3 burden (0.54 %), and marginally decrease in global mean OH (0.08 %). The effect of halving γ is essentially symmetrical, with an increased global tropospheric I_Y burden (4.3 %), increased surface marine boundary layer (900 hPa $< p$) IO concentration (4.3 %), and an increased median bias in vertical comparisons with TORERO aircraft IO by 4.4 to 84 %. This leads to slightly decreased global tropospheric O_3 burden (0.44 %), and marginal increase in OH (0.05 %).

7.7 Summary of sensitivity simulations

Uncertainties in the atmospheric chemistry of iodine lead to some significant uncertainties on iodine's impact on atmospheric composition. Further laboratory studies on the photolytic properties of high oxides would reduce uncertainty, as would a more detailed understanding of the rates of heterogenous cycling on a range of aerosols. The interplay between bromine and iodine chemistry is also potentially significant for the oxidant budgets. Given the inorganic iodine emissions' role as the largest source of iodine into the atmosphere, improved constraints on the concentration of oceanic iodide would also reduce uncertainties. It is clear that we do not have a complete understanding of iodine chemistry in the atmosphere and further laboratory and field observations are necessary to provide a stronger constraint.

8 Conclusions

We have implemented a representation of the tropospheric chemistry of iodine into the GEOS-Chem model and compared it against a range of observational data sets. We estimate a global emission of 3.8 Tg yr^{-1} of iodine, which is consistent with previous work. We find this dominated by the inorganic ocean source (84 %), and the majority (91 %) of deposition is back to the oceans.

Comparisons with the limited IO observational data set shows that the model is within a factor of 2 of the observations on average. Iodine reduces the global tropospheric O_3 burden by ~ 9 %. Global mean OH concentrations are increased (1.8 %) by the presence of iodine due to the reduction in the $O_3 + H_2O$ primary source being compensated for by an increased conversion of HO_2 into OH via the photolysis of HOI. Both changes involve HOI production and destruction cycles.

Our understanding of iodine chemistry is hampered by limited laboratory studies of both its gas and aerosol phase chemistry, by limited field measurements of atmospheric iodine compounds, and poor understanding of ocean surface iodide and its chemistry. Impacts on O_3 and OH are sensitive to the uncertainty of ocean iodine emissions, the parametrization of iodine recycling in aerosol, to the photolysis parameters for the higher oxides, and to the assumed Br chemistry. Given its role as the largest component of atmospheric iodine, and its central role in both O_3 destruction and HO_2 to IO cycling, a priority should be given to instrumentation to measure HOI.

Appendix A

A1 Additional details on sensitivity runs

A1.1 Details of reactions within scheme, but not present within IUPAC/JPL

The field of iodine chemistry is still young, and some reactions that are used within box model/global studies are not in the IUPAC/JPL compilations due to uncertainties in the laboratory studies or for other reasons. Different choices have been made regarding reactions included in previous box model (Bloss et al., 2010; Mahajan et al., 2009; Read et al., 2008; Saiz-Lopez et al., 2008; Sommariva et al., 2012) and global model studies (Breider, 2010; Ordóñez et al., 2012; Saiz-Lopez et al., 2012b, 2014). The following reactions have been included within our simulation's chemistry scheme (Tables 3 and 4) although they are not in the IUPAC/JPL compilations.

$$HOI + OH \rightarrow IO + H_2O \quad \text{(M5)}$$

Uncertainties exist over product channels for this reaction (Sommariva et al., 2012). In our study we assume the products are IO and H_2O based on laboratory experiments (Riffault et al., 2005) and previous box model analysis (Sommariva et al., 2012).

$$INO_3 + I \rightarrow I_2 + NO_3 \quad \text{(M12)}$$

This reaction's rate is based on a single theoretical study (Kaltsoyannis and Plane, 2008). The impact of inclusion within a box model was found to be minimal, except in high iodine and NO_X conditions (Sommariva et al., 2012).

$$OIO + OIO \rightarrow I_2O_4 \quad \text{(M17)}$$

This reaction rate is from a single experimental study (Gómez Martín et al., 2007), which yielded a lower limit of $1.2 \pm 0.3 \times 10^{-10}$ cm^3 molecules^{-1} s^{-1}. This reaction is included in this work, along with the reverse reaction (Reaction M24, $I_2O_4 \rightarrow 2OIO$).

$$INO_3 \xrightarrow{M} IO + NO_2 \quad \text{(M26)}$$

The reaction is included in the IUPAC (Atkinson et al., 2007) without direct experiment observation. No recommendation is given in the recent JPL compilation (Sander et al., 2011). The INO_3 thermal stability used by studies has led to a significant range between reaction rates (298 K) from 1.08×10^{-2} (Read et al., 2008) to 2.51×10^{-5} cm^3 molecules^{-1} s^{-1} (Sommariva et al., 2012). The latter use the most recent theoretical study (Kaltsoyannis and Plane, 2008), which we also use here. The forward reaction (Reaction M25) has been included ubiquitously in iodine modelling work; and the reverse reaction (Reaction M26) is employed in the majority of, but not all studies (Ordóñez et al., 2012). Both reactions are included in this work.

$$IO + OIO \xrightarrow{M} I_2O_3 \quad \text{(M21)}$$

A single experimental study (Gómez Martín et al., 2007) gives a upper limit and lower rate limit of 1.5×10^{-10} and 1.5×10^{-11} cm^3 molecules^{-1} s^{-1}, respectively. We use the higher value in this work as in others studies (Saiz-Lopez et al., 2008; Sommariva et al., 2012).

$$I_2O_2 \xrightarrow{M} IO + IO \quad \text{(M22)}$$

$$I_2O_2 \xrightarrow{M} OIO + I \quad \text{(M23)}$$

These reactions have been studied solely theoretically (Kaltsoyannis and Plane, 2008). A temperature-dependent rate was calculated theoretically (Ordóñez et al., 2012) which is used in our work.

$$I_2O_4 \xrightarrow{M} 2OIO \quad \text{(M24)}$$

The rate is calculated from the value for binding energy of the dimer (Kaltsoyannis and Plane, 2008). As we have included Reaction M17 ($OIO + OIO \rightarrow I_2O_4$), we also include the reverse reaction (M24) in our work at the Kaltsoyannis and Plane (2008) rate.

A1.2 Detail of reactive uptake coefficients (γ) used for heterogeneous reactions

As described in Sect. 3.1, we stoichiometrically emit I_2 following the uptake of species that hydrolyse to HOI (INO_2, INO_3, HOI). We assume this to avoid double counting of Br release already included within the model as described by Parrella et al. (2012). Lack of, or limited experimental data reduces certainty on heterogeneous processing of halogens. The reactive uptake coefficients (γ) used in this study are experimentally constrained wherever possible or follow previously estimated values in the literature as described below.

The JPL compilation notes a single experimental study of HOI uptake on H_2SO_4, yielding mass accommodation coefficients (α) in the range 0.02 to 0.07 (Sander et al., 2011). Another two studies on ice and salt are reported in JPL with lower limits of 0.0022 and 0.01 respectively (Sander et al., 2011). IUPAC evaluates two experimental studies which "concur (the) uptake coefficient is large", but no recommendation is given due to possible uncertainties in reversibility (Crowley et al., 2010). The γ values used in the literature range between 0.01 (Mahajan et al., 2009; Breider, 2010) and 0.5 (Saiz-Lopez et al., 2007). The higher end of this range originates from an investigation of the sensitivity to this parameter by Saiz-Lopez et al. (2007) for which the base case was set as 0.02. A γ value of 0.01 is used within our work.

For INO_2 and INO_3 no experiment work is available on the uptake and values have previously been estimated by analogy with measured equivalent bromine species. For INO_3 a γ

value of 0.01 has been frequently used based on estimations (Mahajan et al., 2009; Ordóñez et al., 2012), but values have been used up to 0.2 (Bloss et al., 2010). For INO_2 γ values of 0.01 (Mahajan et al., 2009) or 0.02 (Ordóñez et al., 2012; Saiz-Lopez et al., 2007) have often been used, but γ values up to 0.1 have also been used (Bloss et al., 2010). In this work γ values of 0.01 and 0.02 are used for INO_3 and INO_2 respectively.

The IUPAC compilation includes a recommendation for HI uptake γ on ice of 0.2 (Crowley et al., 2010), based on three experimental studies. A γ value of 0.1 though has most often been used in modelling studies (Breider, 2010; Mahajan et al., 2009; Saiz-Lopez et al., 2008) and is used in this work.

For I_2O_X ($X = 2, 3, 4$) no experimental data are available for reactive uptake coefficients. The uptake has been discussed in the literature, including a box model study which tested sensitivity around a base value of 0.02 (Saiz-Lopez et al., 2008). The γ value for I_2O_X was set at 0.02 by with analogy INO_2. This value is highly uncertain and values up to 1 have been used for gamma in modelling studies (Bloss et al., 2010). A value of 0.02 is used within this work.

Table A1. Effects of sensitivity runs on relevant variables. Values are shown as percentage change from the simulation with both iodine and bromine chemistry ("Br+I") in the troposphere as global means unless otherwise stated. MBL = Marine Boundary Layer (900 hPa $< p$), O_X is defined as in footnote 1. CH_4 lifetime is calculated globally in the troposphere with respect to loss by reaction with OH.

	Mean IO MBL surface concentration	Chem. O_X loss (LO_X)	Chem. O_X prod. (PO_X)	PO_X -LO_X	O_3 burden	O_3 deposition
NOHAL	−100.00	2.34	−0.75	40.91	15.99	17.75
BROMINE	−100.00	−1.79	−3.90	24.50	9.12	10.42
IODINE	9.63	3.87	2.89	16.16	6.90	6.87
Br+I	0.00	0.00	0.00	0.00	0.00	0.00
Just org. I	−83.45	−1.64	−3.11	17.69	5.53	7.19
I_2O_X loss (γ) ×2	−4.26	−0.15	−0.28	1.61	0.54	0.59
I_2O_X loss (γ)/2	3.93	0.13	0.24	−1.34	−0.44	−0.52
Het. cycle (γ) ×2	2.21	0.04	0.16	−1.61	−0.69	−0.56
Het. cycle (γ)/2	−1.84	−0.06	−0.14	1.07	0.56	0.45
No het. cycle	−48.03	−1.15	−2.20	12.60	4.09	5.23
Sulfate uptake	−22.49	−1.25	−2.26	12.06	4.54	4.94
Ocean iodide	−34.28	−0.66	−1.26	7.24	2.06	3.01
I_2O_X X-sections ×2	4.30	0.11	0.22	−1.34	−0.40	−0.47
I_2O_X exp. X-sections	6.73	0.19	0.35	−1.88	−0.60	−0.73
No I_2O_X photolysis	−39.35	−1.10	−2.12	12.33	5.05	4.86
MBL BrO 2 pmol mol^{-1}	−6.78	−3.59	−2.71	−15.28	−3.73	−6.03

	OH mean concentration	HO_2 mean concentration	HO_2 /OH	I_Y lifetime	IO_X lifetime	I_Y burden	CH_4 lifetime
NOHAL	2.49	8.44	5.81	−100.00	105.16	−100.00	−3.73
BROMINE	−1.65	5.72	7.50	−100.00	89.64	−100.00	0.80
IODINE	4.30	2.31	−1.91	−1.31	−1.82	6.96	−4.67
Br+I	0.00	0.00	0.00	0.00	0.00	0.00	0.00
Just org. I	−0.64	3.53	4.19	123.92	16.09	−64.26	0.21
I_2O_X loss (γ) ×2	−0.08	0.27	0.36	−8.38	−0.93	−5.08	0.03
I_2O_X loss (γ)/2	0.05	−0.22	−0.27	8.00	0.55	4.27	−0.01
Het. cycle (γ) ×2	0.09	−0.39	−0.49	4.61	1.13	5.98	0.00
Het. cycle (γ)/2	−0.09	0.32	0.41	−3.89	−0.96	−5.04	0.02
No het. cycle	−0.47	2.58	3.07	−61.18	5.38	−46.69	0.15
Sulfate uptake	−0.87	2.70	3.60	−59.60	0.49	−48.49	0.52
Ocean iodide	−0.17	1.22	1.39	16.90	2.77	−23.42	0.01
I_2O_X X-sections ×2	0.05	−0.20	−0.25	5.26	0.61	3.10	−0.01
I_2O_X exp. X-sections	0.08	−0.31	−0.39	8.31	0.84	4.81	−0.01
No I_2O_X photolysis	−0.90	2.54	3.48	−46.41	−17.68	−34.58	0.32
MBL BrO 2 pmol mol^{-1}	−3.31	−1.44	1.93	−3.72	3.33	−10.07	4.17

Acknowledgements. This work was funded by NERC quota studentship NE/K500987/1 with support from the NERC BACCHUS and CAST projects NE/L01291X/1, NE/J006165/1.

R. Volkamer acknowledges funding from US National Science Foundation CAREER award ATM-0847793, AGS-1104104, and AGS-1452317. The involvement of the NSF-sponsored Lower Atmospheric Observing Facilities, managed and operated by the National Center for Atmospheric Research (NCAR) Earth Observing Laboratory (EOL), is acknowledged.

T. Sherwen would like to acknowledge constructive comments from and conversations with all coauthors as well as R. Chance and J. Schmidt.

Edited by: M. Uematsu

References

Ainsworth, E. A., Yendrek, C. R., Sitch, S., Collins, W. J., and Emberson, L. D.: The effects of tropospheric ozone on net primary productivity and implications for climate change, Annu. Rev. Plant Bio., 63, 637–661, doi:10.1146/annurev-arplant-042110-103829, 2012.

Alexander, B.: Sulfate formation in sea-salt aerosols: Constraints from oxygen isotopes, J. Geophys. Res., 110, D10307, doi:10.1029/2004JD005659, 2005.

Amos, H. M., Jacob, D. J., Holmes, C. D., Fisher, J. A., Wang, Q., Yantosca, R. M., Corbitt, E. S., Galarneau, E., Rutter, A. P., Gustin, M. S., Steffen, A., Schauer, J. J., Graydon, J. A., Louis, V. L. St., Talbot, R. W., Edgerton, E. S., Zhang, Y., and Sunderland, E. M.: Gas-particle partitioning of atmospheric Hg(II) and its effect on global mercury deposition, Atmos. Chem. Phys., 12, 591–603, doi:10.5194/acp-12-591-2012, 2012.

Andrews, S. J., Jones, C. E., and Carpenter, L. J.: Aircraft measurements of very short-lived halocarbons over the tropical Atlantic Ocean, Geophys. Res. Lett., 40, 1005–1010, doi:10.1002/grl.50141, 2013.

Andrews, S. J., Hackenberg, S. C., and Carpenter, L. J.: Technical Note: A fully automated purge and trap GC-MS system for quantification of volatile organic compound (VOC) fluxes between the ocean and atmosphere, Ocean Sci., 11, 313–321, doi:10.5194/os-11-313-2015, 2015.

Atkinson, R., Baulch, D. L., Cox, R. A., Crowley, J. N., Hampson, R. F., Hynes, R. G., Jenkin, M. E., Rossi, M. J., and Troe, J.: Evaluated kinetic and photochemical data for atmospheric chemistry: Volume III – gas phase reactions of inorganic halogens, Atmos. Chem. Phys., 7, 981–1191, doi:10.5194/acp-7-981-2007, 2007.

Atkinson, R., Baulch, D. L., Cox, R. A., Crowley, J. N., Hampson, R. F., Hynes, R. G., Jenkin, M. E., Rossi, M. J., Troe, J., and Wallington, T. J.: Evaluated kinetic and photochemical data for atmospheric chemistry: Volume IV – gas phase reactions of organic halogen species, J. Phys. Chem. Ref. Data, 8, 4141–4496, 2008.

Bedjanian, Y., Le Bras, G., and Poulet, G.: Kinetic study of the Br + IO, I + BrO and Br + I2 reactions. Heat of formation of the BrO radical, Chem. Phys. Lett., 266, 233–238, doi:10.1016/S0009-2614(97)01530-3, 1997.

Bell, N., Hsu, L., Jacob, D. J., Schultz, M. G., Blake, D. R., Butler, J. H., King, D. B., Lobert, J. M., and Maier-Reimer, E.: Methyl iodide: atmospheric budget and use as a tracer of marine convection in global models, J. Geophys. Res.-Atmos., 107, ACH8.1–ACH8.12, doi:10.1029/2001jd001151, 2002.

Bell, R. P.: The Proton in Chemistry, 2nd Edn., Cornell University Press, 1973.

Bian, H. S. and Prather, M. J.: Fast-J2: accurate simulation of stratospheric photolysis in global chemical models, J. Atmos. Chem., 41, 281–296, doi:10.1023/a:1014980619462, 2002.

Bloss, W. J., Rowley, D. M., Cox, R. A., and Jones, R. L.: Kinetics and products of the IO self-reaction, J. Phys. Chem. A, 105, 7840–7854, doi:10.1021/jp0044936, 2001.

Bloss, W. J., Lee, J. D., Johnson, G. P., Sommariva, R., Heard, D. E., Saiz-Lopez, A., Plane, J. M. C., McFiggans, G., Coe, H., Flynn, M., Williams, P., Rickard, A. R., Fleming, L. Z.: Impact of halogen monoxide chemistry upon boundary layer OH and HO_2 concentrations at a coastal site, Geophys. Res. Lett., 32, L06814, doi:10.1029/2004GL022084, 2005a.

Bloss, W. J., Evans, M. J., Lee, J. D., Sommariva, R., Heard, D. E., and Pilling, M. J.: The oxidative capacity of the troposphere: coupling of field measurements of OH and a global chemistry transport model, Faraday Discuss., 130, 425–436, doi:10.1039/b419090d, 2005b.

Bloss, W. J., Camredon, M., Lee, J. D., Heard, D. E., Plane, J. M. C., Saiz-Lopez, A., Bauguitte, S. J.-B., Salmon, R. A., and Jones, A. E.: Coupling of HO_x, NO_x and halogen chemistry in the antarctic boundary layer, Atmos. Chem. Phys., 10, 10187–10209, doi:10.5194/acp-10-10187-2010, 2010.

Braban, C. F., Adams, J. W., Rodriguez, D., Cox, R. A., Crowley, J. N., and Schuster, G.: Heterogeneous reactions of HOI, ICl and IBr on sea salt and sea salt proxies, Phys. Chem. Chem. Phys., 9, 3136–3148, doi:10.1039/b700829e, 2007.

Breider, T. J.: Coupled Halogen-Sulfur-Aerosol Modelling in a 3D Chemical Transport Model, PhD thesis, University of Leeds, Leeds, 2010.

Butz, A., Bösch, H., Camy-Peyret, C., Chipperfield, M. P., Dorf, M., Kreycy, S., Kritten, L., Prados-Román, C., Schwärzle, J., and Pfeilsticker, K.: Constraints on inorganic gaseous iodine in the tropical upper troposphere and stratosphere inferred from balloon-borne solar occultation observations, Atmos. Chem. Phys., 9, 7229–7242, doi:10.5194/acp-9-7229-2009, 2009.

Carpenter, L. J., MacDonald, S. M., Shaw, M. D., Kumar, R., Saunders, R. W., Parthipan, R., Wilson, J., and Plane, J. M. C.: Atmospheric iodine levels influenced by sea surface emissions of inorganic iodine, Nat. Geosci., 6, 108–111, doi:10.1038/ngeo1687, 2013.

Chameides, W. L. and Davis, D. D.: Iodine: its possible role in tropospheric photochemistry, J. Geophys. Res.-Oceans, 85, 7383–7398, doi:10.1029/JC085iC12p07383, 1980.

Chance, R., Baker, A. R., Carpenter, L., and Jickells, T. D.: The distribution of iodide at the sea surface, Environ. Sci.: Processes Impacts, 16, 1841–1859, doi:10.1039/C4EM00139G, 2014.

Chuck, A. L., Turner, S. M., and Liss, P. S.: Oceanic distributions and air-sea fluxes of biogenic halocarbons in the open ocean, J. Geophys. Res.-Oceans, 110, C10022, doi:10.1029/2004jc002741, 2005.

Crowley, J. N., Ammann, M., Cox, R. A., Hynes, R. G., Jenkin, M. E., Mellouki, A., Rossi, M. J., Troe, J., and Wallington, T. J.: Evaluated kinetic and photochemical data for atmospheric chemistry: Volume V – heterogeneous reactions on solid substrates,

Atmos. Chem. Phys., 10, 9059–9223, doi:10.5194/acp-10-9059-2010, 2010.

Dix, B., Baidar, S., Bresch, J., Hall, S., Schmidt, K., Wang, S.-Y., and Volkamer, R.: Detection of iodine monoxide in the tropical free troposphere, P. Natl. Acad. Sci. USA, 110, 2035–2040, doi:10.1073/pnas.1212386110, 2013.

Fiore, A. M., Naik, V., Spracklen, D. V., Steiner, A., Unger, N., Prather, M., Bergmann, D., Cameron-Smith, P. J., Cionni, I., Collins, W. J., Dalsoren, S., Eyring, V., Folberth, G. A., Ginoux, P., Horowitz, L. W., Josse, B., Lamarque, J.-F., MacKenzie, I. A., Nagashima, T., O'Connor, F. M., Righi, M., Rumbold, S. T., Shindell, D. T., Skeie, R. B., Sudo, K., Szopa, S., Takemura, T., and Zeng, G.: Global air quality and climate, Chem. Soc. Rev., 41, 6663–6683, doi:10.1039/C2CS35095E, 2012.

Fowler, D., Amann, M., Anderson, R., Ashmore, M., Cox, P., Depledge, M., Derwent, D., Grennfelt, P., Hewitt, N., Hov, O., Jenkin, M., Kelly, F., Liss, P., Pilling, M., Pyle, J., Slingo, J., and Stevenson, D.: Ground-level ozone in the 21st century: future trends, impacts and policy implications, Tech. rep., The Royal Society, 2008.

Gómez Martín, J. C., Spietz, P., and Burrows, J. P.: Spectroscopic studies of the I_2/O_3 photochemistry: Part 1: Determination of the absolute absorption cross sections of iodine oxides of atmospheric relevance, J. Photoch. Photobio. A, 176, 15–38, doi:10.1016/j.jphotochem.2005.09.024, 2005.

Gómez Martín, J. C., Spietz, P., and Burrows, J. P.: Kinetic and mechanistic studies of the I_2/O_3 photochemistry, J. Phys. Chem. A, 111, 306–320, doi:10.1021/jp061186c, 2007.

Gómez Martín, J. C., Mahajan, A. S., Hay, T. D., Prados-Roman, C., Ordonez, C., MacDonald, S. M., Plane, J. M. C., Sorribas, M., Gil, M., Mora, J. F. P., Reyes, M. V. A., Oram, D. E., Leedham, E., and Saiz-Lopez, A.: Iodine chemistry in the eastern Pacific marine boundary layer, J. Geophys. Res.-Atmos., 118, 887–904, doi:10.1002/jgrd.50132, 2013.

Großmann, K., Frieß, U., Peters, E., Wittrock, F., Lampel, J., Yilmaz, S., Tschritter, J., Sommariva, R., von Glasow, R., Quack, B., Krüger, K., Pfeilsticker, K., and Platt, U.: Iodine monoxide in the Western Pacific marine boundary layer, Atmos. Chem. Phys., 13, 3363–3378, doi:10.5194/acp-13-3363-2013, 2013.

Jacob, D. J.: Heterogeneous chemistry and tropospheric ozone, Atmos. Environ., 34, 2131–2159, doi:10.1016/S1352-2310(99)00462-8, 2000.

Jones, C. E., Hornsby, K. E., Sommariva, R., Dunk, R. M., Von Glasow, R., McFiggans, G., and Carpenter, L. J.: Quantifying the contribution of marine organic gases to atmospheric iodine, Geophys. Res. Lett., 37, L18804, doi:10.1029/2010gl043990, 2010.

Kaltsoyannis, N. and Plane, J. M. C.: Quantum chemical calculations on a selection of iodine-containing species (IO, OIO, INO_3, $(IO)_2$, I_2O_3, I_2O_4 and I_2O_5) of importance in the atmosphere, Phys. Chem. Chem. Phys., 10, 1723–1733, 2008.

Kim, K.-H., Shon, Z.-H., Nguyen, H. T., and Jeon, E.-C.: A review of major chlorofluorocarbons and their halocarbon alternatives in the air, Atmos. Environ., 45, 1369–1382, doi:10.1016/j.atmosenv.2010.12.029, 2011.

Law, K. S. and Sturges, W. T.: Scientific Assessment of Ozone Depletion, 2006 Chapter 2: Halogenated Very Short-Lived Substances, Tech. rep., 2006.

Lawler, M. J., Mahajan, A. S., Saiz-Lopez, A., and Saltzman, E. S.: Observations of I2 at a remote marine site, Atmos. Chem. Phys., 14, 2669–2678, doi:10.5194/acp-14-2669-2014, 2014.

Lelieveld, J. and Dentener, F. J.: What controls tropospheric ozone?, J. Geophys. Res.-Atmos., 105, 3531–3551, doi:10.1029/1999JD901011, 2000.

Liu, H., Jacob, D. J., Bey, I., and Yantosca, R. M.: Constraints from 210Pb and 7Be on wet deposition and transport in a global three-dimensional chemical tracer model driven by assimilated meteorological fields, J. Geophys. Res.-Atmos., 106, 12109–12128, doi:10.1029/2000JD900839, 2001.

MacDonald, S. M., Gómez Martín, J. C., Chance, R., Warriner, S., Saiz-Lopez, A., Carpenter, L. J., and Plane, J. M. C.: A laboratory characterisation of inorganic iodine emissions from the sea surface: dependence on oceanic variables and parameterisation for global modelling, Atmos. Chem. Phys., 14, 5841–5852, doi:10.5194/acp-14-5841-2014, 2014.

Mahajan, A. S., Oetjen, H., Saiz-Lopez, A., Lee, J. D., McFiggans, G. B., and Plane, J. M. C.: Reactive iodine species in a semi-polluted environment, Geophys. Res. Lett., 36, L16803, doi:10.1029/2009GL038018, 2009.

Mahajan, A. S., Plane, J. M. C., Oetjen, H., Mendes, L., Saunders, R. W., Saiz-Lopez, A., Jones, C. E., Carpenter, L. J., and McFiggans, G. B.: Measurement and modelling of tropospheric reactive halogen species over the tropical Atlantic Ocean, Atmos. Chem. Phys., 10, 4611–4624, doi:10.5194/acp-10-4611-2010, 2010.

Mahajan, A. S., Gómez Martín, J. C., Hay, T. D., Royer, S.-J., Yvon-Lewis, S., Liu, Y., Hu, L., Prados-Roman, C., Ordóñez, C., Plane, J. M. C., and Saiz-Lopez, A.: Latitudinal distribution of reactive iodine in the Eastern Pacific and its link to open ocean sources, Atmos. Chem. Phys., 12, 11609–11617, doi:10.5194/acp-12-11609-2012, 2012.

Mao, J., Jacob, D. J., Evans, M. J., Olson, J. R., Ren, X., Brune, W. H., Clair, J. M. St., Crounse, J. D., Spencer, K. M., Beaver, M. R., Wennberg, P. O., Cubison, M. J., Jimenez, J. L., Fried, A., Weibring, P., Walega, J. G., Hall, S. R., Weinheimer, A. J., Cohen, R. C., Chen, G., Crawford, J. H., McNaughton, C., Clarke, A. D., Jaeglé, L., Fisher, J. A., Yantosca, R. M., Le Sager, P., and Carouge, C.: Chemistry of hydrogen oxide radicals (HO_x) in the Arctic troposphere in spring, Atmos. Chem. Phys., 10, 5823–5838, doi:10.5194/acp-10-5823-2010, 2010.

Mao, J., Paulot, F., Jacob, D. J., Cohen, R. C., Crounse, J. D., Wennberg, P. O., Keller, C. A., Hudman, R. C., Barkley, M. P., and Horowitz, L. W.: Ozone and organic nitrates over the eastern United States: sensitivity to isoprene chemistry, J. Geophys. Res.-Atmos., 118, 11256–11268, doi:10.1002/jgrd.50817, 2013.

McFiggans, G., Plane, J. M. C., Allan, B. J., Carpenter, L. J., Coe, H., and O'Dowd, C.: A modeling study of iodine chemistry in the marine boundary layer, J. Geophys. Res.-Atmos., 105, 14371–14385, doi:10.1029/1999JD901187, 2000.

McFiggans, G., Bale, C. S. E., Ball, S. M., Beames, J. M., Bloss, W. J., Carpenter, L. J., Dorsey, J., Dunk, R., Flynn, M. J., Furneaux, K. L., Gallagher, M. W., Heard, D. E., Hollingsworth, A. M., Hornsby, K., Ingham, T., Jones, C. E., Jones, R. L., Kramer, L. J., Langridge, J. M., Leblanc, C., LeCrane, J.-P., Lee, J. D., Leigh, R. J., Longley, I., Mahajan, A. S., Monks, P. S., Oetjen, H., Orr-Ewing, A. J., Plane, J. M. C., Potin, P., Shillings, A. J. L., Thomas, F., von Glasow, R., Wada, R., Whalley, L. K., and Whitehead, J. D.: Iodine-mediated coastal particle formation:

an overview of the Reactive Halogens in the Marine Boundary Layer (RHaMBLe) Roscoff coastal study, Atmos. Chem. Phys., 10, 2975–2999, doi:10.5194/acp-10-2975-2010, 2010.

McLinden, C. A., Olsen, S. C., Hannegan, B., Wild, O., Prather, M. J., and Sundet, J.: Stratospheric ozone in 3-D models: a simple chemistry and the cross-tropopause flux, J. Geophys. Res., 105, 14653, doi:10.1029/2000JD900124, 2000.

Murray, B. J., Haddrell, A. E., Peppe, S., Davies, J. F., Reid, J. P., O'Sullivan, D., Price, H. C., Kumar, R., Saunders, R. W., Plane, J. M. C., Umo, N. S., and Wilson, T. W.: Glass formation and unusual hygroscopic growth of iodic acid solution droplets with relevance for iodine mediated particle formation in the marine boundary layer, Atmos. Chem. Phys., 12, 8575–8587, doi:10.5194/acp-12-8575-2012, 2012.

Ordóñez, C., Lamarque, J.-F., Tilmes, S., Kinnison, D. E., Atlas, E. L., Blake, D. R., Sousa Santos, G., Brasseur, G., and Saiz-Lopez, A.: Bromine and iodine chemistry in a global chemistry-climate model: description and evaluation of very short-lived oceanic sources, Atmos. Chem. Phys., 12, 1423–1447, doi:10.5194/acp-12-1423-2012, 2012.

Parrella, J. P., Jacob, D. J., Liang, Q., Zhang, Y., Mickley, L. J., Miller, B., Evans, M. J., Yang, X., Pyle, J. A., Theys, N., and Van Roozendael, M.: Tropospheric bromine chemistry: implications for present and pre-industrial ozone and mercury, Atmos. Chem. Phys., 12, 6723–6740, doi:10.5194/acp-12-6723-2012, 2012.

Prados-Roman, C., Cuevas, C. A., Fernandez, R. P., Kinnison, D. E., Lamarque, J.-F., and Saiz-Lopez, A.: A negative feedback between anthropogenic ozone pollution and enhanced ocean emissions of iodine, Atmos. Chem. Phys., 15, 2215–2224, doi:10.5194/acp-15-2215-2015, 2015a.

Prados-Roman, C., Cuevas, C. A., Hay, T., Fernandez, R. P., Mahajan, A. S., Royer, S.-J., Galí, M., Simó, R., Dachs, J., Großmann, K., Kinnison, D. E., Lamarque, J.-F., and Saiz-Lopez, A.: Iodine oxide in the global marine boundary layer, Atmos. Chem. Phys., 15, 583–593, doi:10.5194/acp-15-583-2015, 2015.

Puentedura, O., Gil, M., Saiz-Lopez, A., Hay, T., Navarro-Comas, M., Gómez-Pelaez, A., Cuevas, E., Iglesias, J., and Gomez, L.: Iodine monoxide in the north subtropical free troposphere, Atmos. Chem. Phys., 12, 4909–4921, doi:10.5194/acp-12-4909-2012, 2012.

Read, K. A., Mahajan, A. S., Carpenter, L. J., Evans, M. J., Faria, B. V. E., Heard, D. E., Hopkins, J. R., Lee, J. D., Moller, S. J., Lewis, A. C., Mendes, L., McQuaid, J. B., Oetjen, H., Saiz-Lopez, A., Pilling, M. J., and Plane, J. M. C.: Extensive halogen-mediated ozone destruction over the tropical Atlantic Ocean, Nature, 453, 1232–1235, doi:10.1038/nature07035, 2008.

Riffault, V., Bedjanian, Y., and Poulet, G.: Kinetic and mechanistic study of the reactions of OH with IBr and HOI, J. Photoch. Photobio. A, 176, 155–161, doi:10.1016/j.jphotochem.2005.09.002, 2005.

Saiz-Lopez, A., Plane, J. M. C., McFiggans, G., Williams, P. I., Ball, S. M., Bitter, M., Jones, R. L., Hongwei, C., and Hoffmann, T.: Modelling molecular iodine emissions in a coastal marine environment: the link to new particle formation, Atmos. Chem. Phys., 6, 883–895, doi:10.5194/acp-6-883-2006, 2006.

Saiz-Lopez, A., Chance, K., Liu, X., Kurosu, T. P., and Sander, S. P.: First observations of iodine oxide from space, Geophys. Res. Lett., 34, L12812, doi:10.1029/2007gl030111, 2007.

Saiz-Lopez, A., Plane, J. M. C., Mahajan, A. S., Anderson, P. S., Bauguitte, S. J.-B., Jones, A. E., Roscoe, H. K., Salmon, R. A., Bloss, W. J., Lee, J. D., and Heard, D. E.: On the vertical distribution of boundary layer halogens over coastal Antarctica: implications for O_3, HO_x, NO_x and the Hg lifetime, Atmos. Chem. Phys., 8, 887–900, doi:10.5194/acp-8-887-2008, 2008.

Saiz-Lopez, A., Lamarque, J.-F., Kinnison, D. E., Tilmes, S., Ordóñez, C., Orlando, J. J., Conley, A. J., Plane, J. M. C., Mahajan, A. S., Sousa Santos, G., Atlas, E. L., Blake, D. R., Sander, S. P., Schauffler, S., Thompson, A. M., and Brasseur, G.: Estimating the climate significance of halogen-driven ozone loss in the tropical marine troposphere, Atmos. Chem. Phys., 12, 3939–3949, doi:10.5194/acp-12-3939-2012, 2012a.

Saiz-Lopez, A., Plane, J. M. C., Baker, A. R., Carpenter, L. J., von Glasow, R., Martin, J. C. G., McFiggans, G., and Saunders, R. W.: Atmospheric chemistry of iodine, Chem. Rev., 112, 1773–1804, doi:10.1021/cr200029u, 2012b.

Saiz-Lopez, A., Fernandez, R. P., Ordóñez, C., Kinnison, D. E., Gómez Martín, J. C., Lamarque, J.-F., and Tilmes, S.: Iodine chemistry in the troposphere and its effect on ozone, Atmos. Chem. Phys., 14, 13119–13143, doi:10.5194/acp-14-13119-2014, 2014.

Sander, R.: Compilation of Henry's law constants (version 4.0) for water as solvent, Atmos. Chem. Phys., 15, 4399–4981, doi:10.5194/acp-15-4399-2015, 2015.

Sander, R., Vogt, R., Harrris, G. W., and Crutzen, P. J.: Modelling the chemistry of ozone, halogen compounds, and hydrocarbons in the arctic troposphere during spring, Tellus B, 49, 522–532, doi:10.1034/j.1600-0889.49.issue5.8.x, 1997.

Sander, S. P., Golden, D. M., Kurylo, M. J., Moortgat, G. K., Wine, P. H., Ravishankara, A. R., Kolb, C. E., Molina, M. J., Finlayson-Pitts, B. J., Huie, R. E., and Orkin, V. L.: Chemical kinetics and photochemical data for use, in: Atmospheric Studies Evaluation, Number 15, 2006.

Sander, S. P., Friedl, R. R., Abbatt, J. P. D., Barker, J. R., Burkholder, J. B., Golden, D. M., Kolb, C. E., Kurylo, M. J., Moortgat, G. K., Wine, P. H., Huie, R. E., and Orkin, V. L.: Chemical kinetics and photochemical data for use in atmospheric studies, Evaluation Number 17, Tech. rep., NASA Jet Propulsion Laboratory, 2011.

Sofen, E. D. and Evans, M. J.: Surface O_3 dataset, Earth Syst. Sci. Data Discuss., in preparation, 2015.

Sommariva, R., Bloss, W. J., and von Glasow, R.: Uncertainties in gas-phase atmospheric iodine chemistry, Atmos. Environ., 57, 219–232, doi:10.1016/j.atmosenv.2012.04.032, 2012.

Spietz, P., Gómez Martín, J. C., and Burrows, J. P.: Spectroscopic studies of the I_2/O_3 photochemistry: Part 2. Improved spectra of iodine oxides and analysis of the IO absorption spectrum, J. Photoch. Photobio. A, 176, 50–67, doi:10.1016/j.jphotochem.2005.08.023, 2005.

Stuart, A. L. and Jacobson, M. Z.: A timescale investigation of volatile chemical retention during hydrometeor freezing: non-rime freezing and dry growth riming without spreading, J. Geophys. Res., 108, 4178, doi:10.1029/2001JD001408, 2003.

Vogt, R., Sander, R., Von Glasow, R., and Crutzen, P. J.: Iodine chemistry and its role in halogen activation and ozone loss in the marine boundary layer: a model study, J. Atmos. Chem., 32, 375–395, doi:10.1023/a:1006179901037, 1999.

Volkamer, R., Baidar, S., Campos, T. L., Coburn, S., DiGangi, J. P., Dix, B., Eloranta, E. W., Koenig, T. K., Morley, B., Ortega, I., Pierce, B. R., Reeves, M., Sinreich, R., Wang, S., Zondlo, M. A., and Romashkin, P. A.: Aircraft measurements of BrO, IO, glyoxal, NO_2, H_2O, O_2–O_2 and aerosol extinction profiles in the tropics: comparison with aircraft-/ship-based in situ and lidar measurements, Atmos. Meas. Tech., 8, 2121–2148, doi:10.5194/amt-8-2121-2015, 2015.

von Glasow, R., Sander, R., Bott, A., and Crutzen, P. J.: Modeling halogen chemistry in the marine boundary layer 2. Interactions with sulfur and the cloud-covered MBL, J. Geophys. Res.-Atmos., 107, 4323, doi:10.1029/2001JD000943, 2002.

von Glasow, R., von Kuhlmann, R., Lawrence, M. G., Platt, U., and Crutzen, P. J.: Impact of reactive bromine chemistry in the troposphere, Atmos. Chem. Phys., 4, 2481–2497, doi:10.5194/acp-4-2481-2004, 2004.

Voulgarakis, A., Naik, V., Lamarque, J.-F., Shindell, D. T., Young, P. J., Prather, M. J., Wild, O., Field, R. D., Bergmann, D., Cameron-Smith, P., Cionni, I., Collins, W. J., Dalsøren, S. B., Doherty, R. M., Eyring, V., Faluvegi, G., Folberth, G. A., Horowitz, L. W., Josse, B., MacKenzie, I. A., Nagashima, T., Plummer, D. A., Righi, M., Rumbold, S. T., Stevenson, D. S., Strode, S. A., Sudo, K., Szopa, S., and Zeng, G.: Analysis of present day and future OH and methane lifetime in the ACCMIP simulations, Atmos. Chem. Phys., 13, 2563–2587, doi:10.5194/acp-13-2563-2013, 2013.

Wang, S.-Y., Schmidt, J., Baidar, S., Coburn, S., Dix, B., Koenig, T., Apel, E., Bowdalo, D., Campos, T., Eloranta, E., Evans, M., DiGangii, J., Zondlo, M., Gao, R.-S., Haggerty, J., Hall, S., Hornbrook, R., Jacob, D., Morley, B., Pierce, B., Reeves, M., Romashkin, P., ter Schure, A., and Volkamer, R.: Active and widespread halogen chemistry in the tropical and subtropical free troposphere, P. Natl. Acad. Sci. USA, 112, 9281–9286, doi:10.1073/pnas.1505142112, 2015.

Wesely, M. L.: Parameterization of surface resistances to gaseous dry deposition in regional-scale numerical models, Atmos. Environ., 23, 1293–1304, doi:10.1016/0004-6981(89)90153-4, 1989.

WOUDC: WOUDC Ozone Monitoring Community, World Meteorological Organization-Global Atmosphere Watch Program (WMO-GAW)/World Ozone and Ultraviolet Radiation Data Centre (WOUDC) [Data], doi:10.14287/10000001, available at: http://www.woudc.org, last access: 1 October 2014.

Young, P. J., Archibald, A. T., Bowman, K. W., Lamarque, J.-F., Naik, V., Stevenson, D. S., Tilmes, S., Voulgarakis, A., Wild, O., Bergmann, D., Cameron-Smith, P., Cionni, I., Collins, W. J., Dalsøren, S. B., Doherty, R. M., Eyring, V., Faluvegi, G., Horowitz, L. W., Josse, B., Lee, Y. H., MacKenzie, I. A., Nagashima, T., Plummer, D. A., Righi, M., Rumbold, S. T., Skeie, R. B., Shindell, D. T., Strode, S. A., Sudo, K., Szopa, S., and Zeng, G.: Preindustrial to end 21st century projections of tropospheric ozone from the Atmospheric Chemistry and Climate Model Intercomparison Project (ACCMIP), Atmos. Chem. Phys., 13, 2063–2090, doi:10.5194/acp-13-2063-2013, 2013.

Ziska, F., Quack, B., Abrahamsson, K., Archer, S. D., Atlas, E., Bell, T., Butler, J. H., Carpenter, L. J., Jones, C. E., Harris, N. R. P., Hepach, H., Heumann, K. G., Hughes, C., Kuss, J., Krüger, K., Liss, P., Moore, R. M., Orlikowska, A., Raimund, S., Reeves, C. E., Reifenhäuser, W., Robinson, A. D., Schall, C., Tanhua, T., Tegtmeier, S., Turner, S., Wang, L., Wallace, D., Williams, J., Yamamoto, H., Yvon-Lewis, S., and Yokouchi, Y.: Global sea-to-air flux climatology for bromoform, dibromomethane and methyl iodide, Atmos. Chem. Phys., 13, 8915–8934, doi:10.5194/acp-13-8915-2013, 2013.